To investigate the tensile deformation behavior of high martensite DP steels using nano-indentation and spherical indentation hardness testing

A Dissertation submitted

in fulfillment of the requirements

for the Degree of

Master of Engineering

in

Production Engineering

By

VIKRAM JEET

Regd. No. 801685019

Under Supervision of:

Dr. Tarun Nanda
Associate Professor, MED
TIET, Patiala

Dr. B. Ravi Kumar
Sr. Principal Scientist, MTE
CSIR-NML, Jamshedpur

MECHANICAL ENGINEERING DEPARTMENT
THAPAR INSTITUTE OF ENGINEERING AND TECHNOLOGY
(A DEEMED TO BE UNIVERSITY), PATIALA-147004, PUNJAB, India
JULY, 2018

CERTIFICATE

I, Vikram Jeet, hereby declare that the work presented in this thesis entitled **"To investigate the tensile deformation behavior of high martensite DP steels using nano-indentation and spherical indentation hardness testing"** in fulfillment of the requirements for the award of degree of Master of Engineering (Production Engineering) submitted to Mechanical Engineering Department, **Thapar Institute of Engineering and Technology, Patiala** is an authentic record of work carried out under the supervision of **Dr. Tarun Nanda**, Associate Professor, MED, TIET, Patiala and **Dr. B. Ravi Kumar,** Senior Principal Scientist, CSIR-NML, Jamshedpur from July 2016–2018. The matter presented in this report has not been submitted either in part or full to any other university or institute for the award of any degree.

(Vikram Jeet)

Date: 10.08.2018

Dr. Tarun Nanda
Associate Professor
Mechanical Engineering Department
TIET, Patiala

Dr. B. Ravi Kumar
Senior Principal Scientist
MTE Division
CSIR-NML, Jamshedpur

ACKNOWLEDGEMENT

I would like to express my deepest sense of gratitude and a very sincere thanks to my guides Dr. Tarun Nanda, Associate Professor, Mechanical Engineering Department, Thapar Institute of Engineering and Technology, Patiala and Dr. B. Ravi Kumar**,** Senior Principal Scientist, CSIR-NML, Jamshedpur for their sincere and invaluable guidance and full support which helped me in the accomplishment of this thesis report in the present form. Their dynamic and diligent enthusiasm has been highly instrumental in keeping my spirits high. Their flawless and forthright suggestions blended with an innate intelligent application have crowned my task with success.

I also acknowledge the opportunity given to me for training at *National Metallurgical Laboratory*. My special thanks to all the technical staff of CSIR-NML, Jamshedpur for their ready assistance during my experimentation phase.

I am also thankful to Dr. T.P Singh, Head of Department, Mechanical Engineering, for providing us with the adequate infrastructure for carrying out the work. I would like to thank the entire faculty and staff of Mechanical Engineering Department and my friends who devoted their valuable time and helped me in all possible ways towards successful completion of this work.

Lastly, I would like to thank my family for their years of guidance, support, and encouragement. It would not have been possible without them to reach up to this point. They have always wanted the best for me and I admire their determination and sacrifices.

VIKRAM JEET

ABSTRACT

Dual phase steels find extensive applications in auto-industry because of their characteristic properties. For the ferrite-martensite dual phase steels, the soft phase (ferrite) imparts ductility whereas the hard phase (martensite) imparts strength. Ferrite affects the properties mainly through its volume fraction whereas martensite affects the properties by its volume fraction as well as morphology and distribution. In the present work, the starting steel of low carbon content was processed through CAS route with slight changes resulting in two harmonic type dual phase microstructures (core and shell type). These steels containing DP microstructures had differences in martensite fraction and grain size and were designated as DP-1 and DP-2 steels. Volume fraction of martensite in DP-1 and DP-2 was 52.2% and 62.2% respectively. After tensile tests, it was found that DP-2 resulted in more ultimate tensile strength, yield strength, and ductility. Reasons for difference in the tensile properties of the two steels were investigated with SEM analysis of fractured surfaces of tensile tested specimens. The deformation behaviour/damage mechanisms shown by the two steels were also analyzed using nano-indentation and spherical indentation hardness testing techniques. For nano-indentation hardness testing, contour plots were plotted for hardness under constant low load as well as progressive load (low to high load conditions) at various locations. Spherical indentation hardness testing was also done to confirm the outcomes of nano-indentation hardness testing results. Here, plots were made for hardness as a function of depth of indentation. It was found that in DP-1 steel, hardness didn't change significantly at various points of testing (contour plots did not show significant change in color pattern at different locations). However, in DP-2 steel, contour plots showed significant changes in colour at various points of observation. The results of hardness testing showed that for DP-2 steel showing better tensile properties, both the phases (i.e. ferrite as well as martensite) participated in the plastic deformation process. The same trend was also found in spherical indentation which showed that in DP-2 steel, both the phases accommodated plastic deformation, thus provided superior strength-ductility combination.

Keywords: Dual phase steels, harmonic structure, contour plots, nano-indentation, spherical indentation.

TABLE OF CONTENTS

LIST OF FIGURES

LIST OF TABLES

NOMENCLATURE

Acronym	Full Form
AHSS	Advance High Strength Steel
DP	Dual Phase
YS	Yield Strength
UTS	Universal Tensile Strength
TRIP	Transformation Induced Plasticity
TWIP	Twin Induced Plasticity
CP	Complex Phase
Q-P	Quenching Partitioning
MVF	Martensite Volume Fraction
IHT	Inter-critical Holding Temperature
CAS	Core and Shell
SEM	Scanning Electron Microscopy
TEM	Transmission Electron Microscopy
EBSD	Electron Back Scatter Diffraction
GNDs	Geometrically Necessary Dislocations
LVDT	Linear Variable Differential Transformer
CAL	Continuous Annealing Line
CHCL	Continuous Heating and Cooling Line
PAT	Peak Annealing Temperature

CHAPTER 1

INTRODUCTION

1.1 General

This chapter introduces the concept of new generation steels called ‘Advanced High Strength Steels (AHSS). The classification of these steels is discussed. Special focus has been made on dual phase steels (DP steels). The processing routes used for DP steels have also been discussed. In the present dissertation work, the role of hardness measurement in determining tensile deformation behavior of DP steels has been discussed. So, in the last section of the chapter nano-indentation hardness measurement and spherical indentation hardness measurement have been discussed.

1.2 Advanced High Strength Steels

Advanced high strength steels (AHSS) provide good strength along with good ductility. AHSS provide Steels having yield strength and ultimate tensile strength greater than 350 MPa and 550 MPa respectively are called AHSS [1–4]. Figure 1.1 presents various AHSS depicting strength-ductility combinations.

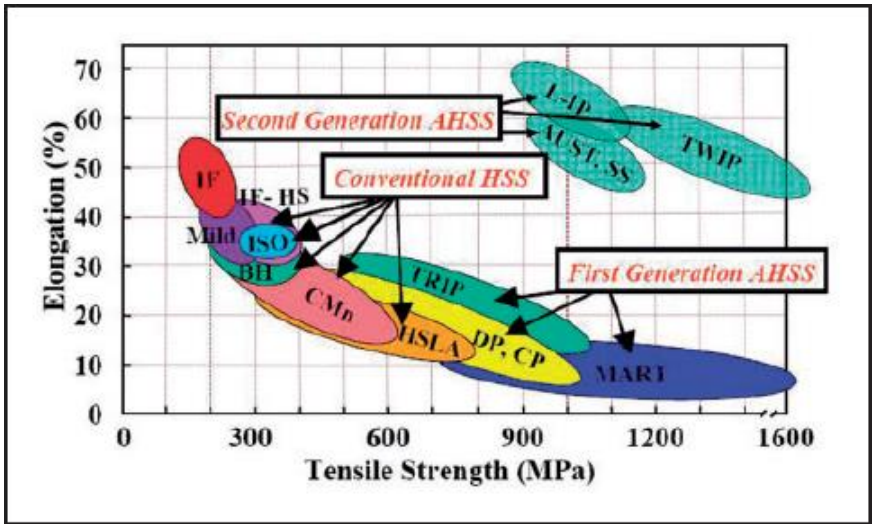

Figure 1.1 Various AHSS with combination of ductility and tensile strength [1–4].

AHSS contain carbon in the range of 0.05–0.2% C, manganese in the range of 1.2–1.6%, and silicon in the range of 0.03–0.6% Si. Small additions (maximum: 0.1%) vanadium, niobium, and titanium are also present. AHSS can be processed by a classical heat treatment process,

constituting of austenizing at a temperature higher than Ac_1 of the steel followed by holding and finally quenching. The typical phases present in AHSS are ferrite, retained austenite, bainite, and martensite.

1.3 Classification of AHSS

AHSS are classified as follows:

- **First Generation or conventional AHSS:** When product of tensile strength and percentage elongation is lower than 25000 MPa than it comes under first generation steels. The main drawbacks of these steels include limited deformation and toughness. These include dual phase steels, complex phase steels, and transformations induced plasticity steels [5–9].
- **Second Generation AHSS:** These steels contain large amount of alloying elements to improve their formability. These have good strength and ductility. This category of AHSS includes light–weight induced plasticity steels, twin induced plasticity steels, shear band formation induced plasticity steels. These steels are excessively alloyed (Mn, Ni, Si, Al, P, Cr). Since these alloying elements are expensive, the cost of production of these steels is very high [8–11].
- **Third Generation AHSS:** This category of steels is currently under development. Third generation is being developed to overcome the main drawbacks of earlier two generations. This generation is extension of first generation steels (this category includes modified DP, TRIP, and CP steels). Superior strength and ductility combination is imparted by varying the processing routes and improving grain refinement. [8, 10, 11].

1.4 Dual Phase Steels

Dual phase steels (or DP steels) possess good combination of mechanical properties. In DP steels, this combination is achieved by obtaining a ferrite/bainite or ferrite/martensite microstructure. For ferrite/martensite DP steels, ferrite forms the soft matrix with 10–40% of martensite phase. DP steels tensile strengths in the range of 400–1000 MPa [8, 10, 11].

1.5 Processing of Dual Phase Steels

A given steel alloy can be transformed to DP steel by using an appropriate processing route (heating, holding, and quenching). The steel is heated up to the full or inter-critical temperature where pearlite is transformed to austenite, held at that temperature, followed by quenching. During quenching the austenite is transformed to martensite. Martensite volume fraction

(MVF) obtained in DP microstructure is dependent on the cooling rate, annealing temperature, and soaking time. The selection of processing routes is dependent on MVF requirements [4].

1.6 Types of annealing routes to get different DP microstructures

To obtain DP microstructure with required phase fraction of constituent phases/desired morphology and distribution of phases, different annealing routes are followed. Routes might differ in the annealing temperatures, heating rates, cooling rates, holding times etc. CAL (Continuous annealing line) is the conventional industrially used process in industry to produce DP steels. Modifications in the heating stage in CAL process results in CHCL (continuous heating and cooling line) route [32,33]. Another route recently developed for improved properties is the CAS route. These annealing routes are presented in Figure 1.2.

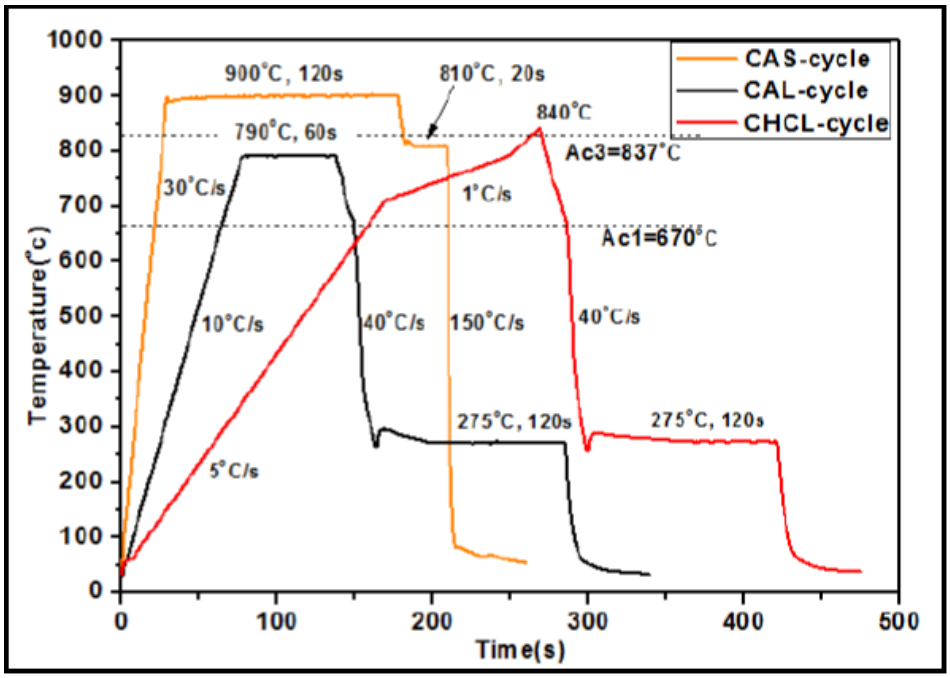

Figure 1.2 Temperature-time plot representing different annealing routes of CAL, CHCL, and CAS [32].

a) Continuous annealing line (CAL) route

The specimen is heated at rate of 10 ℃/s up to 790 ℃, is held at this temperature of 60 s. Holding at this temperature is done to form and grain growth of austenite. Cooling is done in three stages which differ in cooling rate used under same atmospheric conditions. Cooling stages serve different purposes. First cooling stage results in carbon enrichment of austenite, second stage avoids the formation of bainite, and third stage imparts ductility by tempering.

b) Continuous heating and cooling line (CHCL) route

This process involves slight modifications in the heating stage of the conventional CAL route to bring changes in the morphology of martensite present in the DP microstructure. Specimen is heated up to 710 ℃ at heating rate of 5 ℃/s to get more recrystallization and dispersion of carbide before reaching the inter-critical temperature. In the second stage, specimen is heated up to 790 ℃ at heating rate of 1 ℃/s. No holding time is provided at this stage as used in CAL process. Third stage involves further heating to 840 ℃ at a heating rate of 2 ℃/s to get same amount of austenite. After heating is completed in these three stages, cooling is done in a manner similar to CAL route.

c) Core and shell (CAS) route

This annealing route gets its name because of the core and shell type microstructure (also called harmonic structure) that it produces in the processed steel. This route was obtained by some modifications to the annealing cycle as reported by Kumar *et al.* [33]. The modifications include heating up to austenitizing temperature of 900 ℃ and holding for time of 120 s. After holding the specimen, it is cooled to 810 ℃ with the objective to obtain core and shell like DP microstructure. After this, ultra-fast cooling rate of 150 ℃/s was used for cooling the specimen to room temperature. Figure 1.2 shows the CAS process. The complete transformation of austenite to martensite was obtained by using ultra-fast cooling rates.

Thus, by heat treating the as-received steel samples by using above discussed three different annealing cycles, it is possible to get DP microstructures with different martensite volume fraction, morphology, and distribution.

1.7 Nano-indentation hardness testing

Nano-indentation hardness testing is used to evaluate properties of materials at the nano-scale. Load versus displacement data is generated through this testing procedure. This data is utilized to determine properties viz. hardness, modulus of elasticity etc. of the material under investigation. The test can also be used to estimate properties of ultra-thin films. So, properties which can generally not be evaluated using conventional methods can be determined through nano-indentation testing. The indenter used generally for this testing is the ‘Berkovich tip’. The indentor material is diamond (see Figure 1.3).

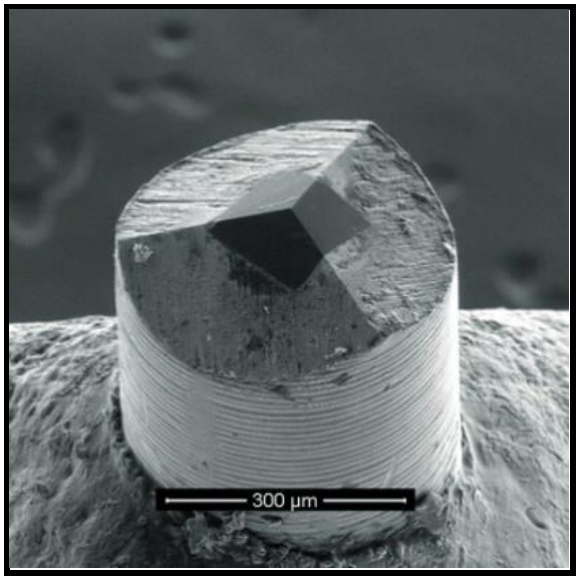

Figure 1.3 Berkovich tip used nano-indentation [29].

Berkovich triangular pyramid (included half-angle of 65.3°) is preferred over Vickers/Knoop indenter. It has three-sided pyramid which can be easily ground to a sharp point.

1.8 Spherical indentation hardness testing

Spherical indentation is similar to nano-indentation with the difference that indenter used is spherical in shape and indenter material is tungsten carbide. Load applied on the specimen is up to 3.5 kN. The diameter of spherical indenter varies from 0.5–1.5 mm. This technique can also be used to find modulus of elasticity and hardness.

1.9 Summary of the chapter

Previous section introduced the concept of AHSS with emphasize on DP steel. The properties and applications of AHSS steels have been discussed. Nano-indentation and spherical indentation techniques has been applied for testing DP steels for micro structural participation in resisting deformation. CAS (core and shell) microstructure can be formed with annealing route different from conventional method used in industry. Next section will discuss related work done by several authors which are related to present work.

CHAPTER 2

LITERATURE REVIEW

2.1 International Status

Delince *et al*. [27] studied the variation of hardness with respect to depth of indentation in DP steel. Experiments were conducted at different loads and for different grain sizes of ferrite and martensite phases. Tests were conducted on nano-indentation machine with Berkovich indenter (see Table 2.1 for steel chemistry).

Table 2.1 Chemical composition of the starting material.

C	Mn	Si	Nb
0.15	1.7	0.5	0.012

Table 2.2 represents the micro-constituent details.

Table 2.2 Volume fraction and grain size details.

	d_f (μm)	d_m (μm)	V_m (%)
CG	3.9	1.4	22
FG	1.0	0.82	26
VFG	0.7	0.87	34

Samples were un-loaded at different forces of 0.25, 0.5, 1, 2, 4, 8 and 12 mN. Loading and un-loading curves of the ferrite and martensite are shown in Figure 2.1.

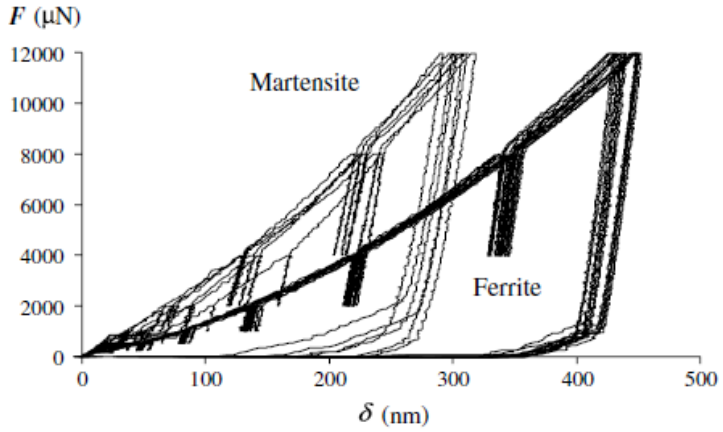

Figure 2.1 Loading-unloading displacement curves for ferrite and martensite for coarse grained sample [27].

It was found that in all the three samples, hardness first decreased, reached a minimum point, and then again started to rise due to strain gradient plasticity effect as shown in Figure 2.2.

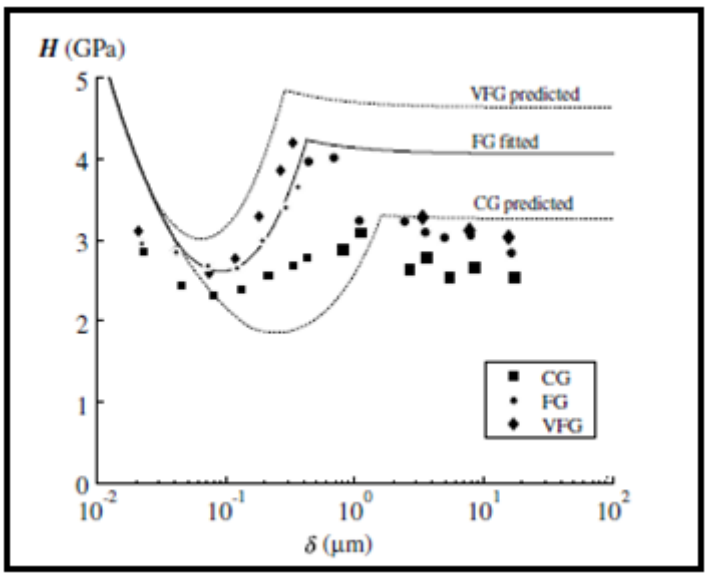

Figure 2.2 Hardness versus depth plot of coarse, fine, and very fine grained specimens [27].

Also, very fine grained sample showed low indentation at the same load as compared to fine and coarse grained specimens (as is also stated by the Hall-Petch equation).

Leitner *et al.* [28] studied three different loading/un-loading methods for two materials (viz. Ni and Cr) to determine their sensitivity towards measurement techniques utilized. The first method called continuous stiffness measurement (CSM) method was performed at a maximum depth of 2500 nm. In CSM, the tool reached a maximum depth of 2500 nm with continuous and repeated vibrations (frequency: 45 Hz, and amplitude: 2 nm). In the second method called the load controlled (LC) method, 8 un-loadings were done till a maximum depth of 2500 nm. In the third method, only 1 un-loading at 2500 nm was done, thus giving only one hardness value. Figure 2.3 shows the results of tests conducted for nickel and chromium.

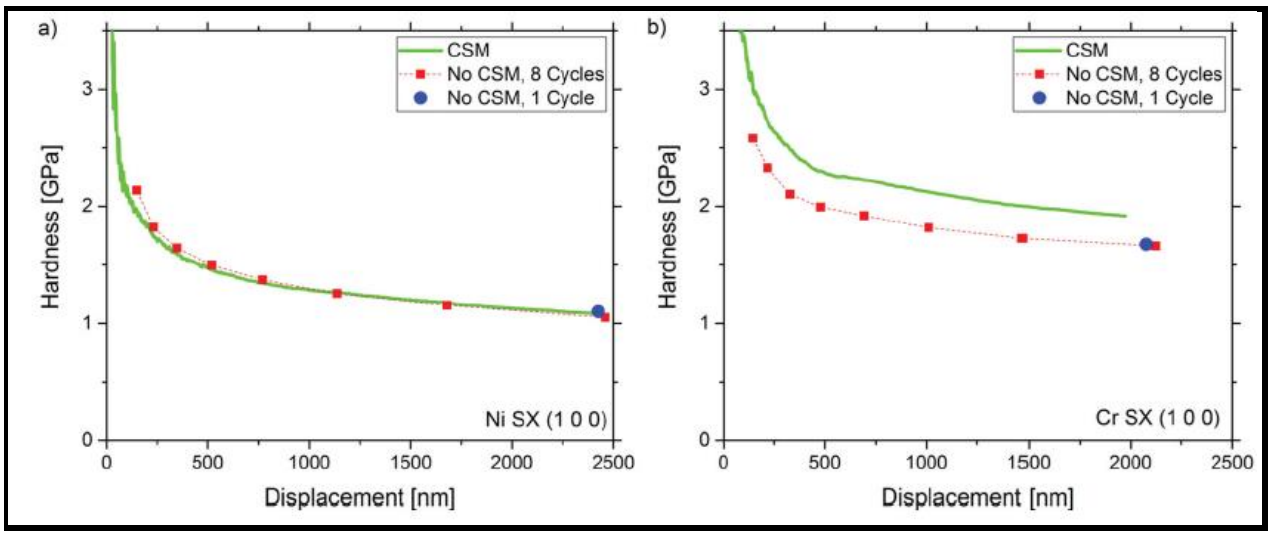

Figure 2.3 Comparison for (a) nickel and (b) chromium at different loadings [28].

Figure 2.2 shows that in case of nickel, CSM and LC methods give similar results without significant difference. However, chromium showed great sensitivity towards the measurement method utilized (loading/un-loading pattern) with significantly different results with CSM and LC methods.

Oliver *et al.* [29] established empirical relations useful to calculate hardness and modulus of elasticity using nano-indentation testing method. Experiments were performed on six different materials including fused silica, soda lime glass, aluminum, tungsten, quartz, and sapphire crystals. Hardness was measured in nano-indentation by a simple relation shown as Equation 2.1.

$$\mathbf{H} = \frac{\boldsymbol{P}}{\boldsymbol{A_C}} \qquad \text{..... (2.1)}$$

Load applied by indenter is 'P' and projected area is 'A_c' after indenter has made indentation into the sample.

Further, the projected cross-sectional area depends directly on the depth of indentation in the sample and is given by the following empirical relation shown as Equation 2.2.

$$\boldsymbol{A_C} = \mathbf{24.5}\ \boldsymbol{h_c^2} \qquad \text{..... (2.2)}$$

$'h_c'$ represents the contact depth.

Further, modulus of elasticity can be found by using the slope of un-loading curve 'S' which can be written as Equation 2.3.

$$\mathbf{S} = \frac{\boldsymbol{dP}}{\boldsymbol{dh}} = \frac{\mathbf{2}\boldsymbol{E_r}\sqrt{\boldsymbol{A_C}}}{\sqrt{\boldsymbol{\pi}}} \qquad \text{..... (2.3)}$$

E_r is the reduced modulus and is given as Equation 2.4.

$$\frac{1}{E_r} = \frac{1-v^2}{E} + \frac{1-v_i^2}{E_i} \qquad \text{..... (2.4)}$$

E and E_i are Young's modulus of elasticity of sample and indenter respectively. v and v_i are Poisson's ratio of sample and indenter respectively. E_i was 1141 GPa and v_i was 0.07 for diamond indenter.

The authors claimed that these empirical equations could determine the hardness and modulus values with accuracy of 5%.

Gavendova *et al.* [30] studied the effect of grain orientation in an electrical grade M 340 steel on the nano-hardness values. Composition of the steel used for experimentation is shown in Table 2.3. Grain orientations obtained in the steel were disturbed by vacuum degassing after final annealing.

Table 2.3 Chemical composition of the steel.

Steel	C (%)	Mn(%)	Si (%)	Cu (%)	P (%)	S (%)	Al (%)	N (%)	Ti (%)
M 340	0.0036	0.183	1.25	0.010	0.039	0.001	0.128	0.0048	0.004

Three grains in different orientations were chosen for nano-indentation. These included G1 [111], G2 [001], and G3 [011]. For each case, twenty indents were made with a gap of 25 μm. Figure 2.4 shows the results of hardness obtained in the three grains with respect to depth of indentation.

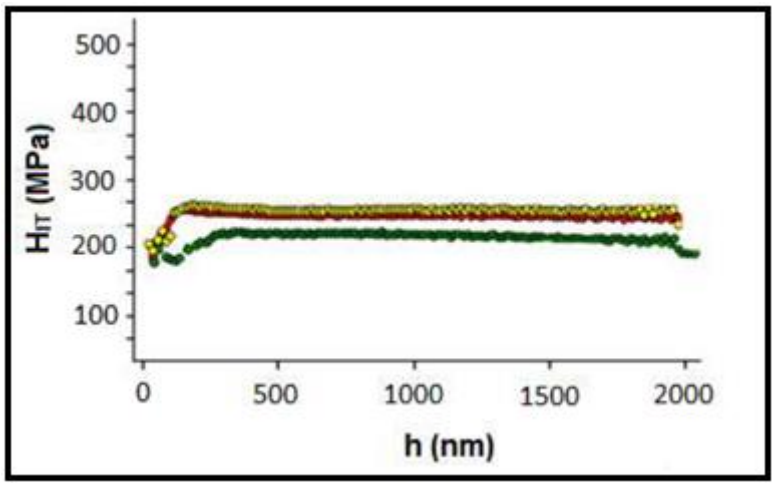

Figure 2.4 Hardness dependence on grain orientation at room temperature [30].

The authors reported that hardness did not show significant dependence on grain orientation when nano-hardness evaluation was done under room temperature conditions.

Challacoop et al. **[31]** studied variation of modulus of elasticity with depth of indentation for hard films formed by vacuum plasma spray process. Thin film of nickel was formed on mirror polished stainless steel specimen. Reduced modulus of elasticity was found using Oliver and Pharr [29] method. Figure 2.5 shows that modulus of elasticity decreases as depth of indentation decreases.

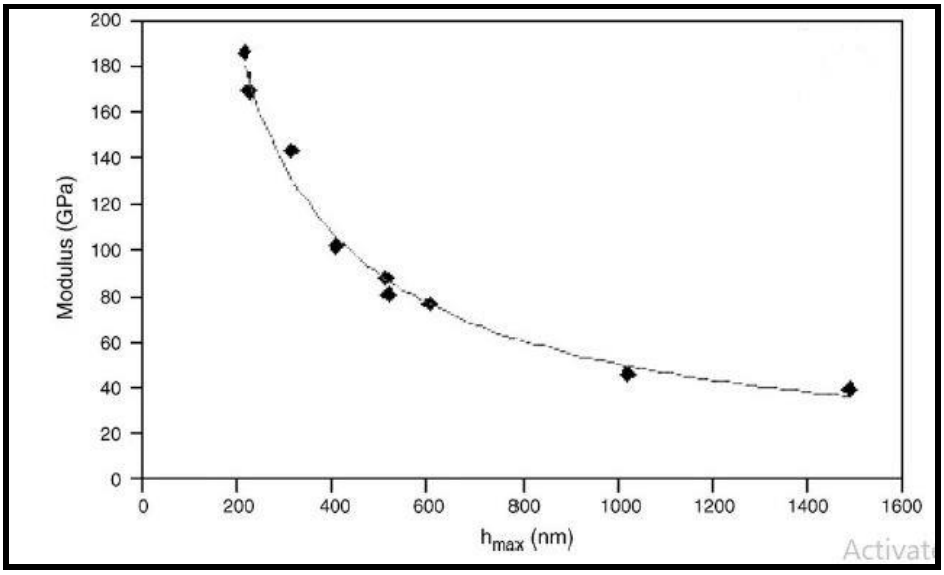

Figure 2.5 Variation of modulus of elasticity with depth of indentation in nickel film [31].

It was observed that modulus reduced to more than 50%, at higher depths of indentation. This was due to the fact that substrate which quite softer than the nickel film. Stress ratio between the two decided the extent up to which the modulus value reduces. If it is greater than 1, the modulus reduces significantly, otherwise it didn't have much effect on it.

Gronostajski *et al.* **[30]** studied the influence of high strain rate loading on the tensile deformation and microstructure in three different types of AHSS. Three grades as shown in Table 2.4 were used for investigation. HC380 was taken as the reference material. For testing under high strain rate conditions, a rotary hammer set-up was used.

Table 2.4 Chemical composition of materials under investigation.

Steel	C [%]	Mn [%]	Si [%]	P [%]	S [%]	Cr [%]	Ni [%]	Al [%]	Fe [%]
HC380	0.16	0.83	0.37	0.014	0.001	0.02	0.01	0.05	Rest
DP600	0.1	1.43	0.19	0.011	0.003	0.028	0.032	0.04	rest
TRIP690	0.14	1.90	0.56	0.005	0.001	0.02	0.01	0.74	rest

Figure 2.6 shows the stress-strain curves of DP600 steel which was tested under various strain rates. At low strain rate, tensile strength was lesser as compared to high strain rates. Also, the area under the curves was more for high strain rate conditions. TRIP690 and HC380 (reference material) also showed similar trends in stress-strain curves. The only difference observed was that DP600 showed highest work hardening even at lower strain rates (followed by HC380 and then TRIP690). Figure 2.7 shows the microstructure of DP600 under different strain rate conditions. In quasi-static loading, void nucleation was observed at martensite-ferrite boundaries which resulted in lower strength. However, under high strain rate conditions, martensite got tempered due to heat accumulation and plastic deformation in the direction of loading.

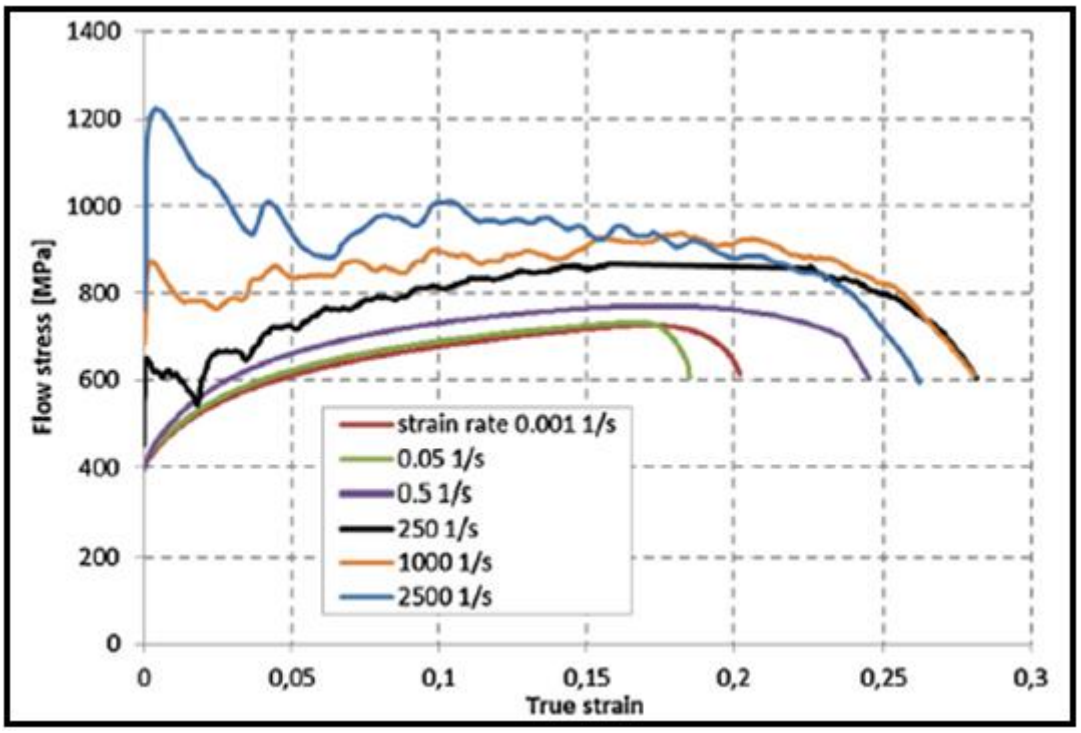

Figure 2.6 True stress-strain curves at different strain rates of DP600 [30].

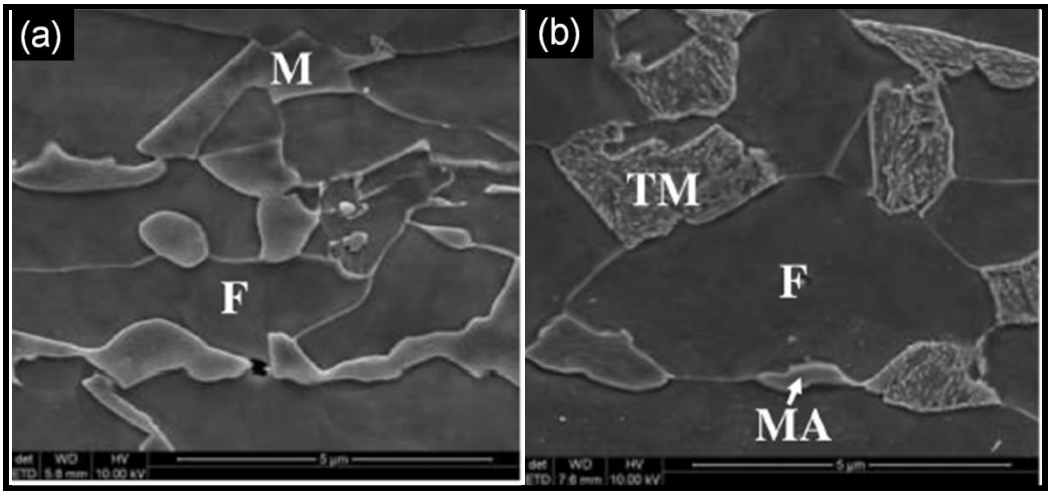

Figure 2.7 SEM micrographs of DP steel under (a) quasi-static loading, (b) high strain rate of 1000 s^{-1} [30].

The reason for high tensile strength under high strain rate condition was due to the fact that strain hardening dominated at low strain rates because of heat loss through conduction and convection. However, at high strain rates, there was no heat loss which caused martensite tempering resulting in high tensile strength.

Uenishi *et al.* [14] investigated strain rate sensitivity of stress and material strengthening by addition of different alloying elements (Si and Mn) to steel. One bar method was utilized to obtain stress-strain diagrams for strain rates greater than 100 s^{-1}. The material behavior at large strains was measured by simple shear tests. It was difficult to evaluate the material behavior by tensile tests due to the onset of necking phenomenon.

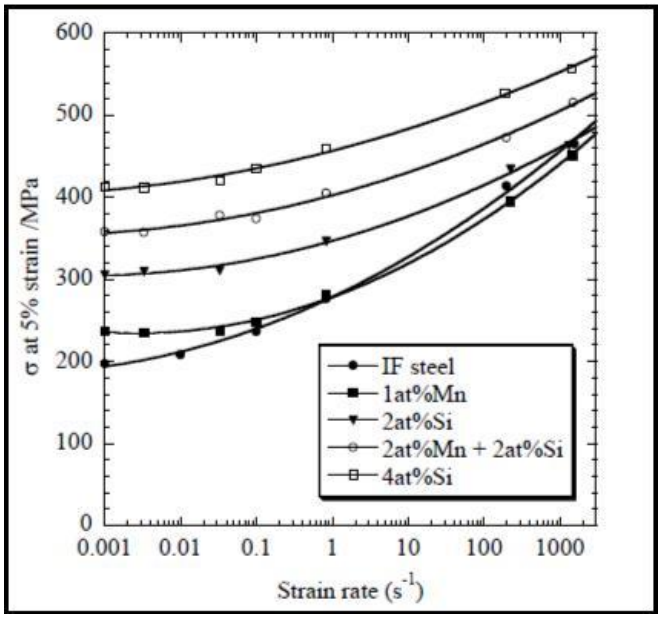

Figure 2.8 True stress versus strain variation at 5% strain [14].

It was observed that for low strain rates, flow stress increased with addition of solute atoms (see Figure 2.8) and strain rate sensitivity of flow stress decreased with quasi-static strength (see Figure 2.9). Multi-phase steels (TRIP steels etc.) showed superior strain rate sensitivity of flow stress.

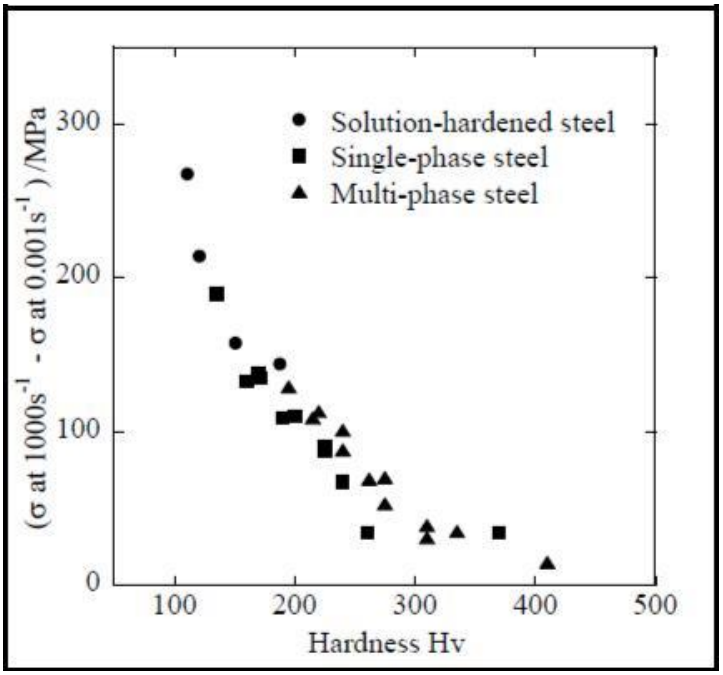

Figure 2.9 Variation of strain rate sensitivity of flow stress with hardness of softer phase [14].

Armaki *et al.* [15] conducted experiments to find deformation behavior of individual phases (martensite/ferrite) with the help of nano-indentation hardness measurements and cylindrical micro-pillars. Steel grade taken for investigation was DP980 processed on CAL. Chemical composition was C-0.15%, Mn-1.45% and Si-0.3%. Thickness of sheet was 2 mm.

Nano-indentation and ion beam milling allowed to measure mechanical properties of different phases. These techniques were used to check the behavior of phases. Figure 2.10 shows the hardness of ferrite phase measured with nano-indentation method. Reading was taken at five different locations out of which one of the readings was taken closer to martensite boundary (here, 1).

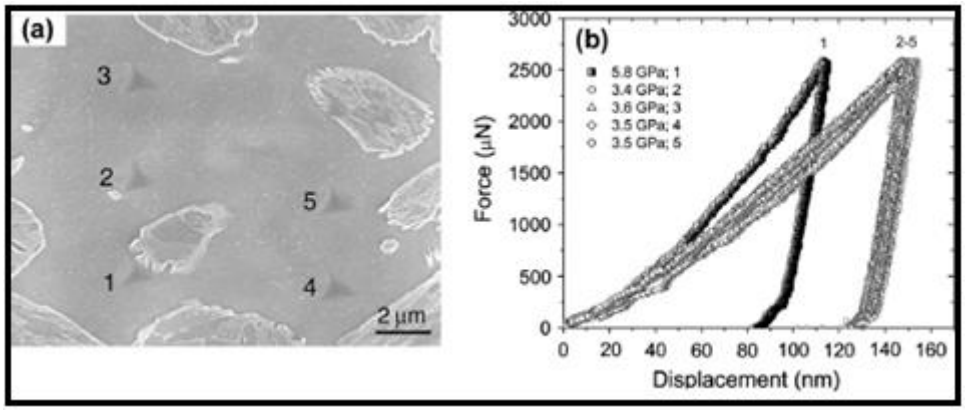

Figure 2.10 (a) Ferrite island selected for checking hardness (b) force displacement curves for ferrite island [15].

Figure 2.10 shows that hardness was maximum (5.8 GPa) for ferrite region which was near to martensite. At other locations (i.e. regions marked as 2–5), hardness ranged between 3.5 ± 0.1 GPa. These observations suggested that harder phase imposes a constraint on the softer phase (here, ferrite) to deform plastically.

Saeidi *et al.* [16] studied the effect of presence of coarse and ultra-fine grains present in DP steel on the yield strength and tensile strength of steel under quasi-static strain rate conditions. Martensitic volume fraction in samples was taken as 50%. Heat treatment processes used in manufacturing of ultra-fine and coarse grained structure are shown in Table 2.5.

Table 2.5 Heat treatment processes applied for manufacturing of different grain sizes in steels.

Designation	Process applied
CG-DP	Annealing at 850 ℃, 20 min. Inter-critical annealing at 740 ℃, 60 min. Finally quenching in water.
UFG-DP	Annealing at 850 ℃, 20 min. Inter-critical annealing at 740 ℃, 60 min. Cold rolling (90%), annealing at 740 ℃ for 3 min. Finally quenching in water.

SEM pictures of the prepared samples are shown in Figure 2.11. The size of CG-DP steel was 5.4 μm and that of UFG-DP steel was 2 μm. Results revealed that there was not much change in yield and tensile strength due to change in grain size but UFG-DP showed more ductility than CG-DP steels. Figure 2.12 shows the engineering stress-strain diagram of the two samples.

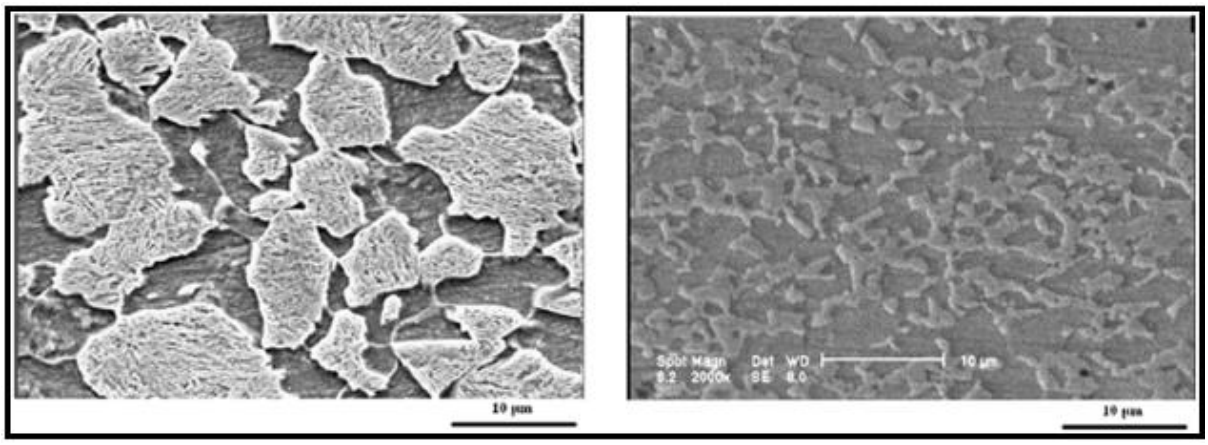

Figure 2.11 SEM micrographs of CG-DP (left) and ultra-fine grained DP steel (right) [16].

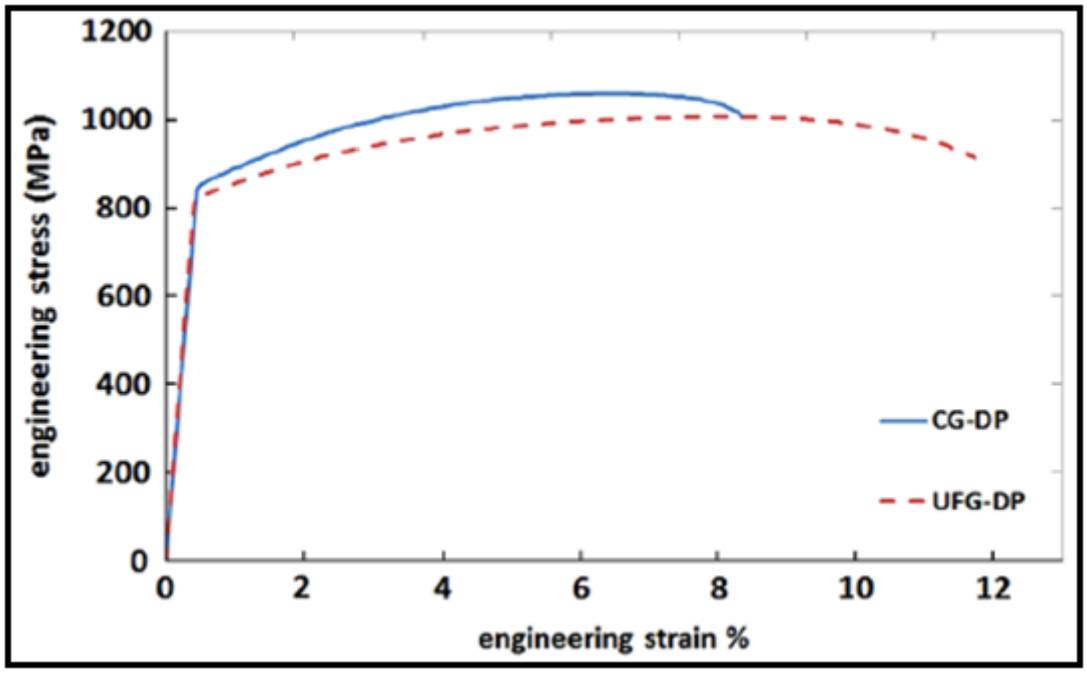

Figure 2.12 Engineering stress strain diagram [16].

Above graph shows that UFG showed increase in ductility but not much change in its tensile and yield behavior. This was due to the fact that in UFG-DP steel martensite phase had round edges as compared to CG-DP steels. So, due to sharp edges of martensite, in CG-DP steels crack initiated at interface boundary between ferrite and martensite which didn't allow martensite to deform up-to its strength, and hence reduced the ductility in CG-DP steels.

Al-Abbasi [25] studied the influence of ferrite grain size/martensite fraction in testing DP steels using micro-mechanical modeling of cells. Ferrite grain sizes of 5, 10, 15, 20, 25, 30, 40, 50, 60 μm were investigated. Volume fraction of martensite taken was 6.8%, 13.7%, 18.5%,

27.8%, and 31.4%. The results of testing are presented in Table 2.6. The effect on uniform elongation and ultimate tensile strength (UTS) was noticed.

Table 2.6 Combined effect of martensite fraction and grain size of ferrite on uniform elongation and UTS.

Ferrite grain size (μm)	V_m = 6.8%		V_m = 13.5%		V_m = 18.5%		V_m = 27.5%		V_m = 31.4%	
	Uniform elongation	UTS (MPa)	Uniform elongation	UTS (MPa)	Uniform elongation	UTS (MPa)	Uniform elongation	UTS (MPa)	Uniform elongation	UTS (MPa)
3	0.118	550.1	0.326	621.1	0.252	687.8	0.159	767.9	0.159	798.4
5	0.130	488.6	0.390	569.2	0.301	637.2	0.183	717.8	0.179	750.1
10	0.330	435.2	0.460	519.8	0.346	588.8	0.224	669.2	0.203	702.8
15	0.350	412.1	0.486	498.7	0.362	568.0	0.248	648.3	0.220	682.2
20	0.362	398.6	0.512	486.5	0.378	555.9	0.256	636.2	0.228	670.3
25	0.374	389.4	0.524	478.3	0.387	547.7	0.265	627.9	0.236	662.2
30	0.383	382.6	0.544	472.3	0.391	541.8	0.273	622.0	0.240	656.3
40	0.391	373.2	0.550	463.9	0.399	533.4	0.281	613.6	0.248	647.9
50	0.399	366.8	0.563	458.3	0.407	527.8	0.285	607.9	0.252	642.3
60	0.407	362.1	0.576	454.2	0.407	523.6	0.289	603.8	0.252	638.2

It was observed that at higher ferrite grain size for any volume fraction of martensite, UTS decreased. It was due to greater ferrite-ferrite interface boundary strength when size of ferrite was finer (finer size restricted motion along its own boundaries which in turn increased the UTS). But there was reduction in ductility (uniform elongation). Low grain size of ferrite at different volume fractions of martensite elongated lesser due to addition in volume of hard phase. As the grain size of ferrite increased, there was increase in ductility for any volume fraction of martensite which suggested ferrite participation during elongation. This was due to reduction in interface boundary strength between ferrite-ferrite boundaries which helped in elongating ferrite, thus overall ductility improved.

Concepcion *et al.* [26] studied influence of carbon amount on microstructure/properties of DP steels. Ferrite-martensite dual phase microstructure was obtained by heating steels (for steel chemistry see Table 2.7) to the inter-critical temperature range followed by water quenching.

Table 2.7 Chemical composition of analyzed materials with critical temperatures.

Material	C	Mn	Si	P	S	Ac_1	Ac_3
S1	0.08	0.77	0.21	0.017	0.012	732	873
S2	0.11	0.69	0.21	0.025	0.021	733	865
S3	0.20	1.45	0.40	0.015	0.028	720	776
S4	0.38	1.43	0.37	0.024	0.033	736	805

Addition of carbon in steels reduced the inter-critical temperature range. It means heat treatment of high carbon steels is more sensitive to temperature variations. Addition of carbon content also increased the amount of martensite formation which is helpful in absorbing shocks.

So, microstructure changes takes place with change in carbon percentage. Mechanical properties also showed some trend with increase in carbon percentage. With increase in carbon percentage, brittleness increased in steels, this reduced ductility of steels. Figure 2.13 shows stress-strain curves of samples with varying carbon percentage.

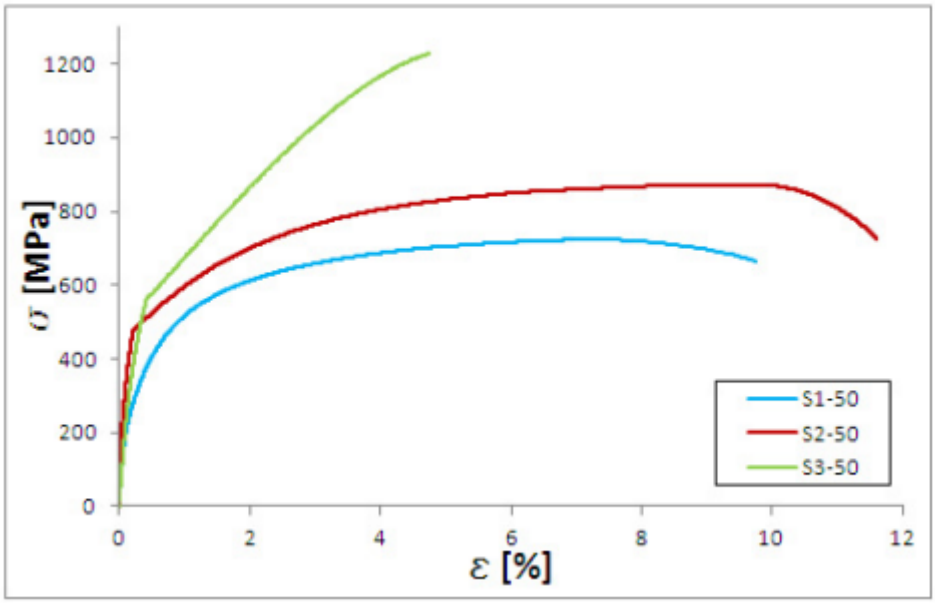

Figure 2.13 Stress-strain diagram of samples with carbon content ranging between 0.08–0.2% [26].

Reduction in elongation was due to greater martensite formation due to more carbon percentage. As the carbon percentage increases, martensite percentage also increases. Martensite is a brittle phase whose failure occurs by crack propagation and it fails suddenly.

Ma *et al.* [36] studied the mechanical properties of nickel coating on carbon steel. Steel sheet of 0.3 mm thickness substrate was used for coating nickel of 3 μm (prepared by electro-depositing method) on both sides of the sheet. Nano-indentation test was carried on two specimens, one with 0% strain and the other with 10% strain (after tensile load application). Progressive loading of both the samples is shown in Figure 2.14. Specimens were loaded up to a maximum depth of 400 nm.

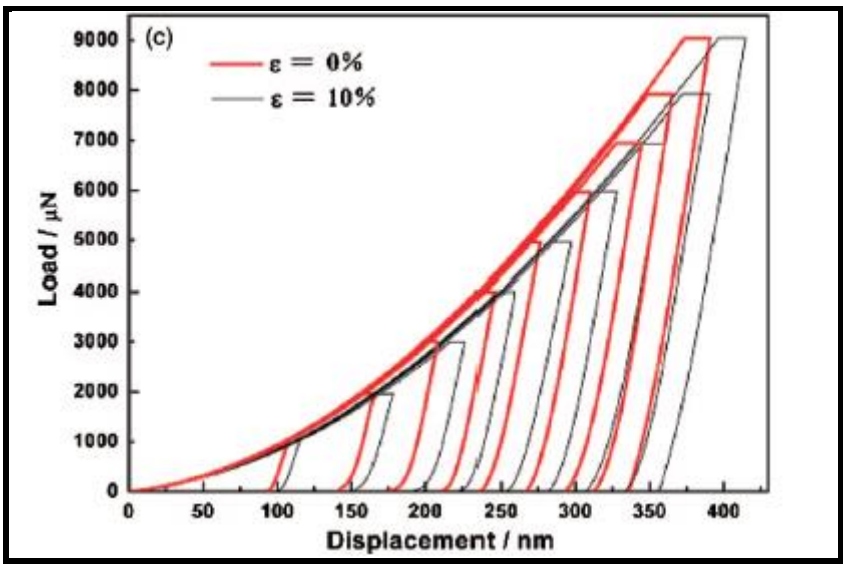

Figure 2.14 Progressive loading in 0% and 10% strained specimen [36].

It was found that hardness decreases with increase in depth of indentation in both the specimens. Graph of hardness versus depth of both the samples are shown in Figure 2.15.

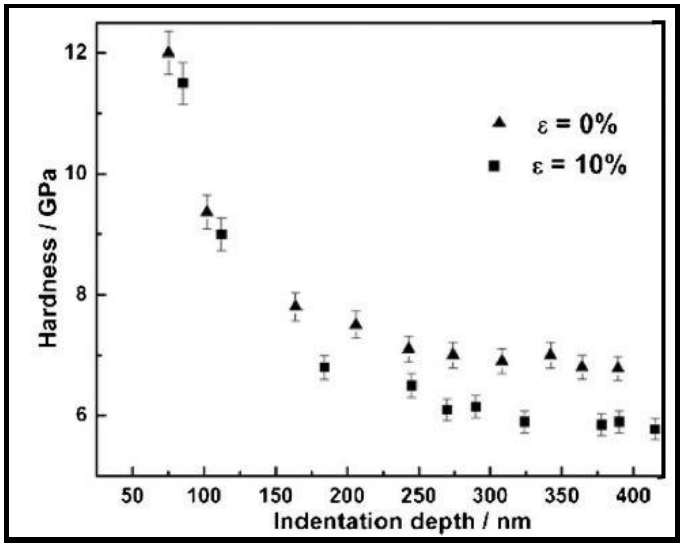

Figure 2.15 Hardness versus depth of indentation plot for specimens [36].

It was observed that nano hardness was more in specimen with 0% strain. The authors reported that in specimen with 10% strain, the hardened steel surface energy reduced after straining.

Apart from above literature there are authors who have worked on indentation size effects on crystalline materials and relate it with geometrically necessary dislocations (GNDs) and burger vector [17]. *Kim et al.* and others have estimated plastic flow properties with the help of nano-indentation like strain hardening exponent[18,19]. *Chen et al.* worked on NiTi (nickel titanium) shape memory alloys (SMA) which possess brilliant wear and corrosion resistant properties and find many applications in industry [20].

National Status

Das *et al.* [21] studied the influence of martensite fraction on the deformation pattern of DP steels. DP600 and DP800 were taken for experimentation work with martensitic volume fraction of 10.2% and 33.2% respectively. The steels were first cold rolled and then annealed for relieving residual stresses. The thickness of steel sheets was 1 mm (see Table 2.8 for steel chemistry). Tensile tests were performed till high rates (800 s^{-1}) on high speed servo-hydraulic test system.

Table 2.8 Chemical composition (in wt. %) of steels.

Material	C	Mn	S	P	Si	Cr	Cu	N (ppm)	Fe
DP600	0.085	0.91	0.008	0.015	0.36	0.022	0.027	30	Bal
DP800	0.11	1.8	0.006	0.016	0.32	0.019	0.021	56	Bal

In DP600, at high strain rate, TEM analysis (see Figure 2.16) showed that ferrite matrix formed a well-defined cell structure. Also, sub-cells were observed. But in DP800 steel, no such type of cell structures were observed, rather it only depicted failure by martensite fragmentation.

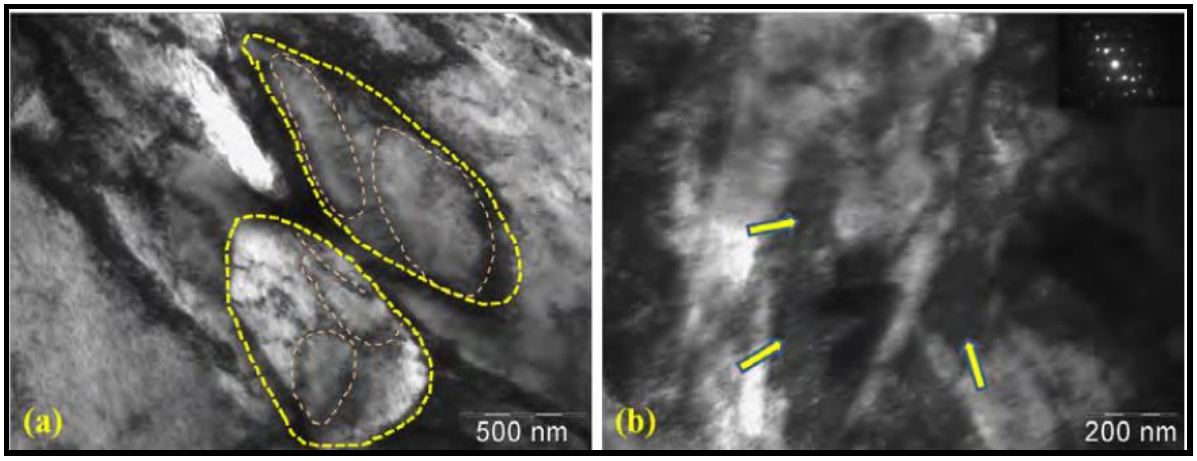

Figure 2.16 (a) DP600 showing cell formation within martensite (b) DP800 showing martensite fragmentation at 800 s^{-1} [21].

Reason for cells formation in DP600 steel only was due to less martensite fraction (10.2%) present in this steel. In DP800, martensitic fraction was 32.2%. It is well established that ferrite yields well before martensite. In DP 600, martensite hardly deforms at all, thus it is only ferrite which deforms and elongates in direction of loading giving rise to strain incompatibility within the two phases which results in void formation at interface boundaries of ferrite and martensite. However, in DP800 steel, martensite resists ferrite rotation within the cells due to its larger volume fraction which results in failure due to martensite fragmentation. The above results

showed that volume fraction of martensite plays an important role in failure of DP steels. In DP600, only ferrite matrix was responsible for failure but in DP800 both ferrite and martensite were preferentially deformed.

Sudersanan *et al.* [22] studied influence on strength with variation of carbon content in second phase martensite present in DP microstructure. Steel chemistry is shown in Table 2.9.

Table 2.9 Steel chemistry of the starting material.

Element	C	Mn	S	P	Si	Cr	Mo	B	Ni
Weight %	0.13	1.18	0.01	0.001	0.3	0.047	0.057	0.001	0.048

The specimens were heat treated in the temperature range of 730–810 ℃. Volume fraction of martensite increased with increase in annealing temperature. Martensite as a hard phase dispersed in soft ferrite matrix provides strength to the dual phase steels, whereas soft ferrite provides ductility. Strength increased initially with martensite volume fraction and then decreased for higher percent of martensite as shown in Fig.2.17a.

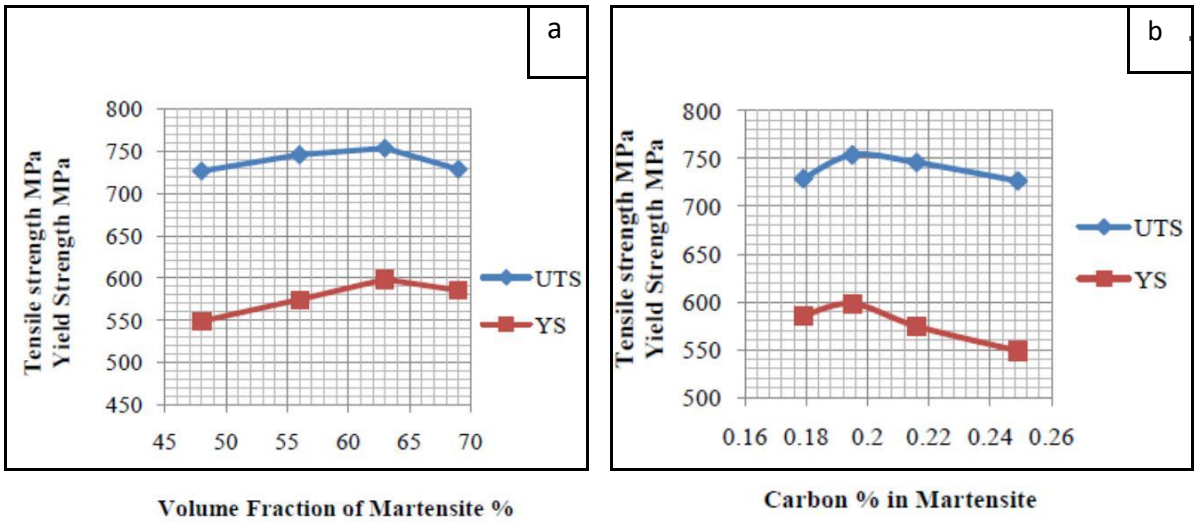

Figure 2.17 (a) Yield and tensile strength v/s volume fraction of martensite (b) yield and tensile strength v/s carbon % in martensite [22].

Carbon content in martensite decreased at higher martensite fraction. YS and UTS increased with increase in carbon content in martensite to a certain limit as shown in Figure 2.14b. YS and UTS were found to increase initially with carbon content up to 0.195 % and then decreased with increase in carbon content in the martensite phase.

Singh *et al.* [32] studied influence of martensite morphology/distribution on strength of specimens processed through three main annealing routes.

Steel chemistry of as-received steel is shown in Table 2.10.

Table 2.10 Steel chemistry of as-received material.

Element	C	Mn	P	S	Si	Al	N
(wt. %)	0.074	1.83	0.012	0.002	0.43	0.026	0.0032

The various annealing routes used by the authors to obtain DP microstructures with differences morphology and distribution of martensite are shown in Figure 2.18.

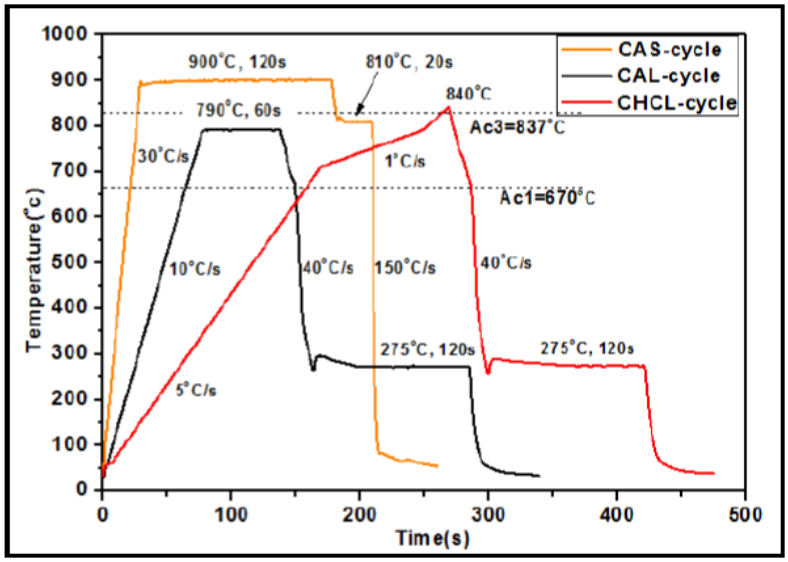

Figure 2.18 Different annealing routes of CAL, CHCL, and CAS used in the research [32].

The annealing route followed for industrial processing of DP steels is the CAL route. The other two routes are modifications over this industrially used process. Continuous annealing line process (CAL route) produced DP microstructure with ferrite as the primary phase (martensite fraction was 20%) with martensite phase mainly present on the grain boundaries of ferrite. The second annealing process called continuous heating and cooling line (CHCL route) produced DP microstructure with same volume fraction of phases (MVF = 20%) as was produced by the CAL route. The main difference between DP microstructures produced by CAL and CHCL was in martensite distribution. For the DP microstructure produced by CHCL route, martensite was present at grain boundaries and also within the ferrite grains (i.e. both grain boundary martensite as well as in-grain martensite were present). The microstructure obtained through 'core and shell' process (CAS route) was quite different. CAS route produced DP microstructure with martensite as the primary phase (martensite fraction was 67%). For this annealing route a typical core and shell type microstructure was obtained. Martensite was present in the core and was surrounded by ferrite channel network which formed the shell of the microstructure. This type of microstructure (core and shell) is typically referred to as

harmonic structure in DP steel literature. The three main types of DP microstructures obtained in the research work as shown in Figure 2.19.

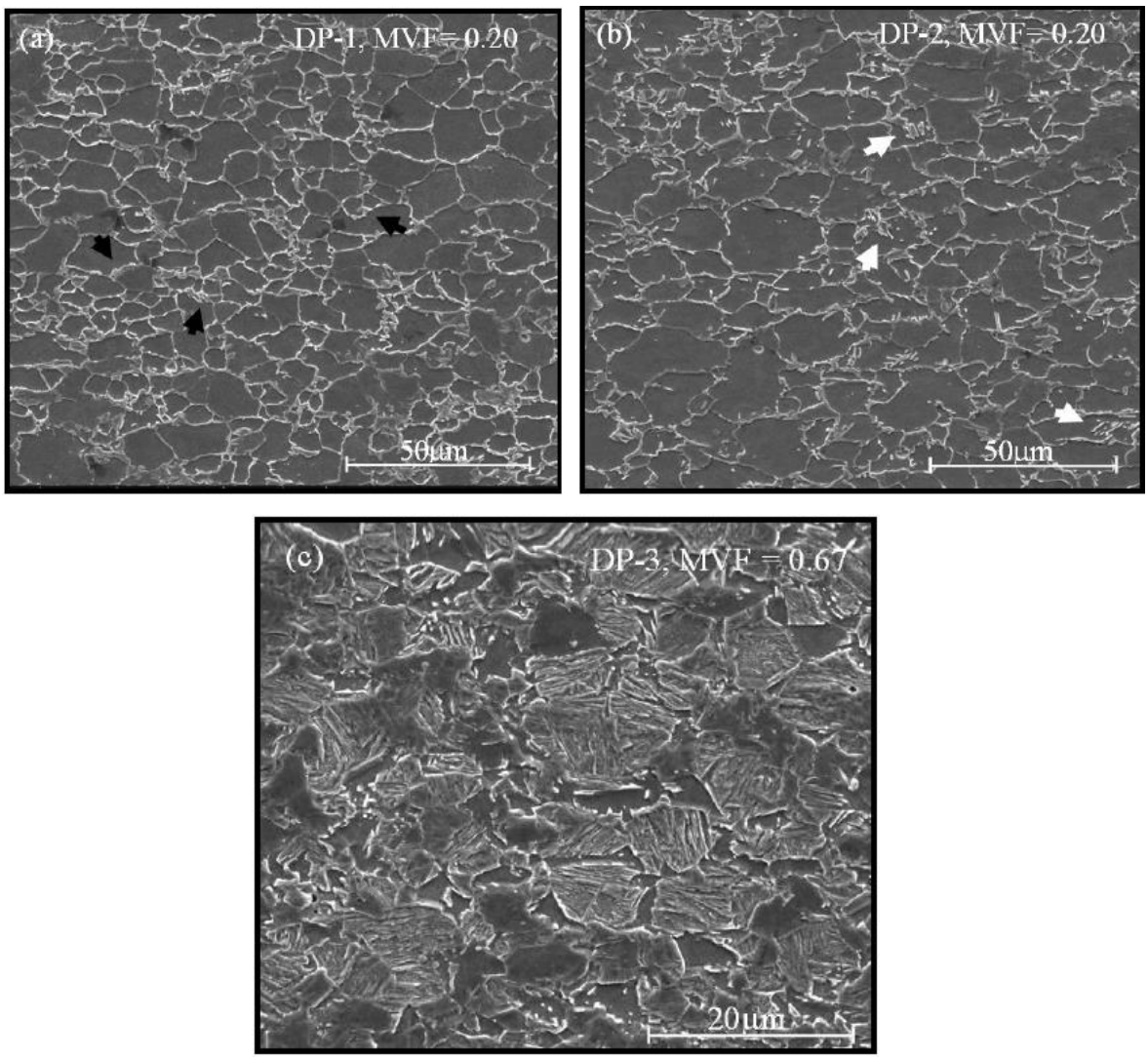

Figure 2.19 SEM micrographs of (a) CAL, (b) CHCL, and (c) CAS processed steels. Black arrows indicate grain boundary martensite and white arrows indicate in-grain martensite [32].

The results of tensile testing are presented in Figure 2.20.

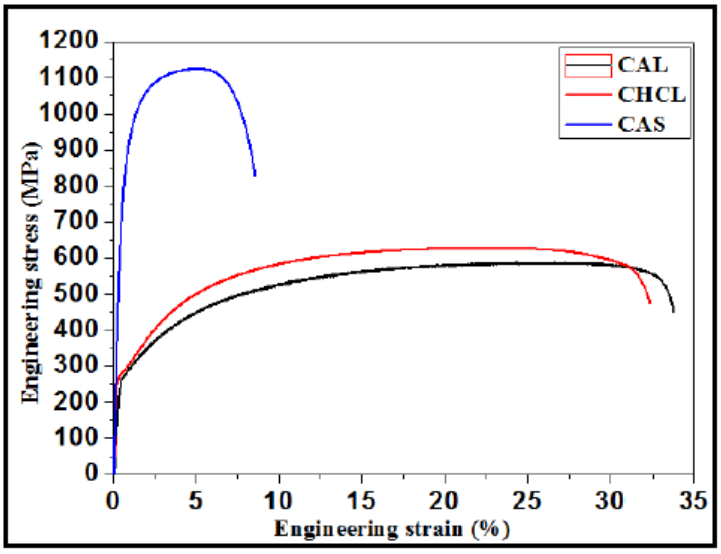

Figure 2.20 Tensile test results for various DP steels [32].

The results showed that CAL and CHCL processed DP steels showed moderate strength with very high ductility. However, the tensile properties of CAS processed steel were very different with very high strength but low ductility.

Kumar *et al.* [33] studied the effect of annealing routes on ferrite channel deposition around martensite phase in DP steels.

The steel chemistry used is shown in Table 2.11.

Table 2.11 Steel chemistry of as-received material [33].

C	Mn	P	S	Si	Al	Cr	N
0.091	1.86	0.014	0.007	0.47	0.038	0.017	0.0035

The various annealing routes followed in the research work are shown in Figure 2.21. Three different peak annealing temperatures (PAT) were used to get three different microstructures. The annealing temperatures were 1000 ℃, 1050 ℃, and 1100 ℃ respectively.

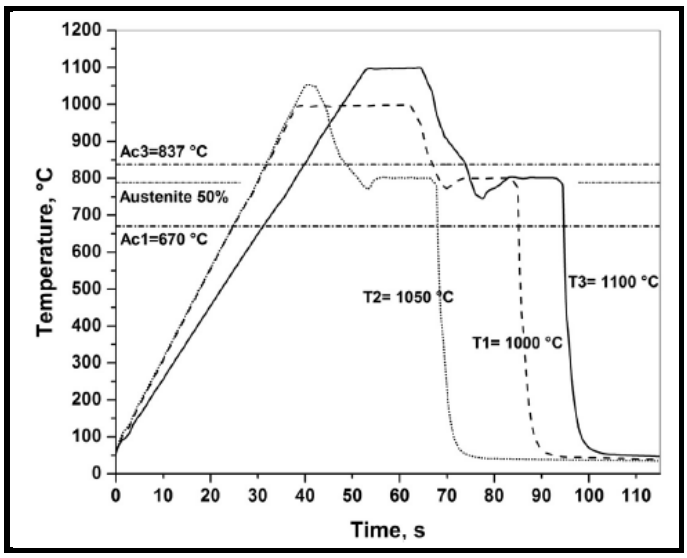

Figure 2.21 Annealing profile used for processing the samples at three different peak temperatures [33].

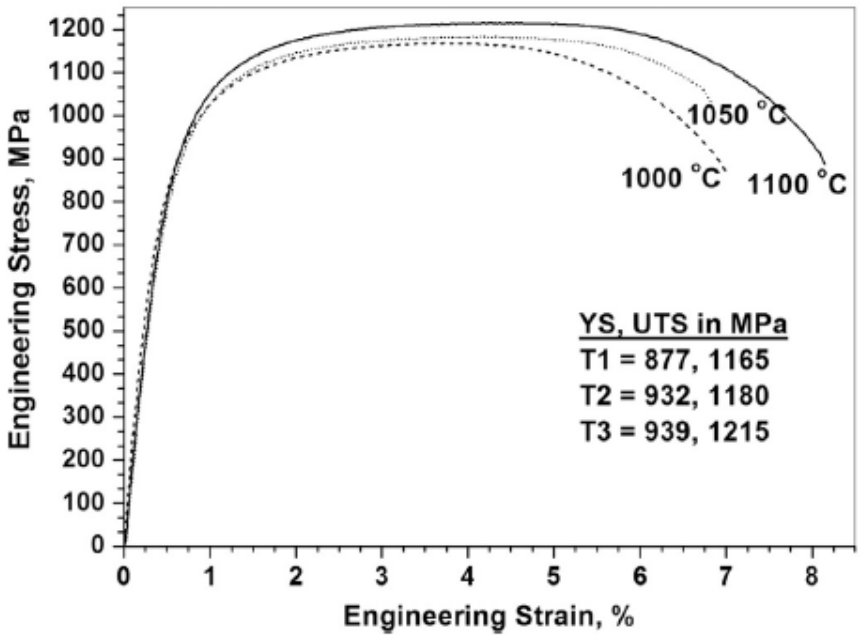

Figure 2.22 Tensile results for three different temperature peaks [33].

The results of tensile testing are presented in Figure 2.22. Core and shell type of microstructure was formed at 1100 ℃ in which soft phase ferrite in the form of a channel network surrounded the martensite phase.

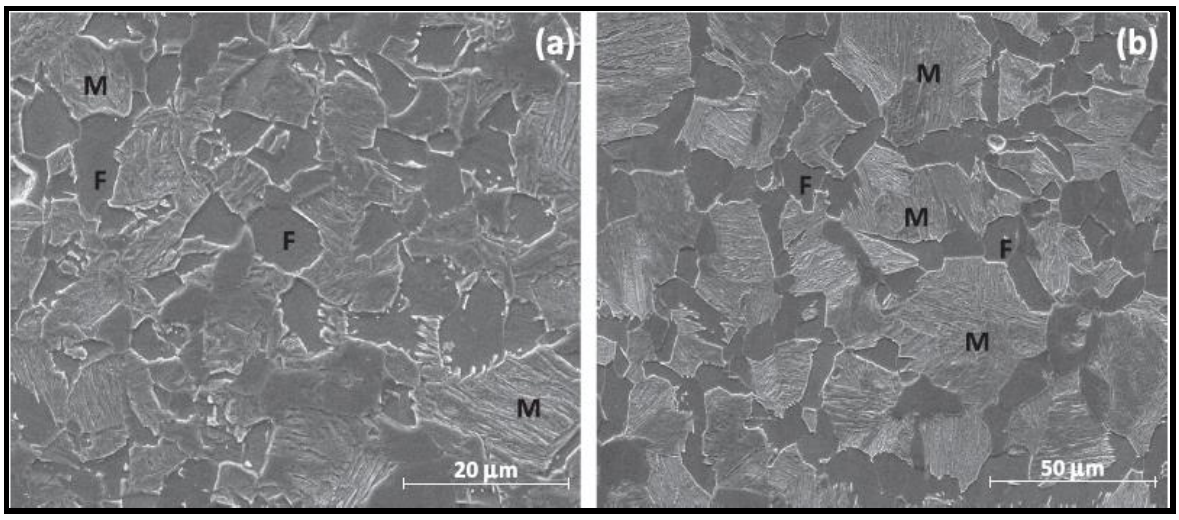

Figure 2.23 DP microstructure obtained through annealing process at (a) 1000 ℃ and ferrite channel formation at (b) 1100 ℃ [33].

The results of tensile testing showed that the core and shell type DP microstructure produced with peak temperature of 1100 ℃ produced the best mechanical properties. For this harmonic structure, the authors reported that inter-lath martensite crack formation was dampened by ferrite shell.

Apart from above literature other authors have work in high strain testing. Ashrafi *et al.* [23] studied the effect of martensite volume fraction, martensite grain size simultaneously by preparing four specimen with different annealing route. Sharma *et al.* [24] simulation study of pearlite to austenite transformation kinetics in rapidly heated hot-rolled low carbon steel.

2.3 Summary of literature

- Some authors have investigated the role of individual phases (ferrite or martensite) present in microstructure on properties of DP steels [15, 16, 21]. Authors have reported that ferrite phase affects the properties of DP steels by virtue of its volume fraction and grain size. Further, martensite phase affects the properties of DP steel by its volume fraction but importantly by its shape and distribution in the DP microstructure [22].
- Further, some authors have investigated the simultaneous effect of martensite fraction along with ferrite grain size on properties of DP steels. It was observed that with increase in ferrite grain size for any martensite fraction, UTS decreased whereas ductility increased [25, 21].
- Authors have worked on various aspects after obtaining results of nano-indentation hardness testing on steels and coatings over other materials. Oliver and Pharr [29] worked on developing empirical relations for modulus of elasticity using nano-indentation

technique. This helped in finding hardness and modulus of elasticity of thin coatings. Nano-hardness studies were also used to obtain hardness versus depth of indentation curves under various conditions (number of loadings/un-loadings, maximum load applied, maximum depth of indentation etc.) to compare differences in properties due to grain size, grain orientation [30].

2.4 Gaps in literature

- Most of the work reported on tensile deformation of DP steels has been for the conventional DP microstructure containing ferrite as the primary phase and containing martensite mainly at ferrite grain boundaries. There is limited work reported in literature on the processing and tensile deformation of harmonic structured DP steels obtained through the 'core and shell' annealing route.
- Limited literature is available on tensile deformation of DP steels (with ferrite-martensite dual phase microstructure) through nano hardness measurements. Though, nano-indentation tests have been utilized to determine properties of thin coated films, this concept has not been widely applied to examine the tensile deformation behavior of DP steels. Nano-indentation and spherical indentation tests can provide insight into participation of micro-constituents of DP microstructure in plastic deformation during tensile testing. This in turn can be used to explain the reasons (from microstructure viewpoint) for the tensile properties displayed by DP steels.

CHAPTER 3

DESIGN OF THE STUDY

3.1 General

The chapter discusses the research objective, key issues, details of starting material, methodology of work, and equipment used in the dissertation work.

3.2 Establishing the objective function

In the present work, two types of dual phase microstructures were produced in the as-received low carbon-low alloy steel for obtaining improved tensile properties. Both the resulting DP steels (referred in the present work as DP-1 and DP-2) contained high martensite fraction and the characteristic harmonic structure (also known as the 'core and shell' type of dual phase microstructure) in which martensite acted as the core and ferrite acted as the shell. The composition of the starting material used for processing of DP-1 and DP-2 steels is shown in Table 3.1.

Table 3.1 Steel chemistry of the starting material.

Element	Mn	Si	C	Al	N	P	S	Fe
Weight Percentage (wt. %)	1.86	0.014	0.091	0.47	0.038	0.035	0.007	Balance

The details of annealing routes used for processing of DP-1 and DP-2 steels are shown in Figure 3.1. Both DP-1 and DP-2 steels contained core and shell type dual phase microstructures but had variations in martensite volume fraction and grain size distribution. Results showed (as are presented in Chapter 4) that DP-2 steel contained higher martensite fraction with relatively finer grain size of martensite phase.

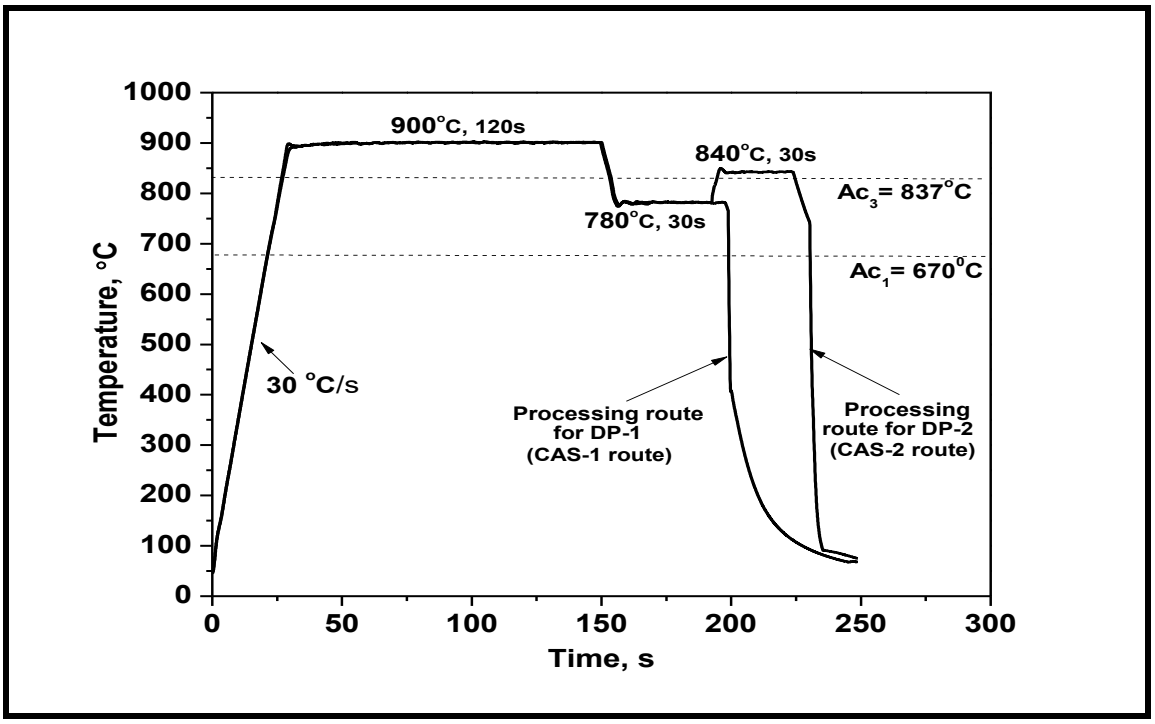

Figure 3.1 Time-temperature profile of annealing processes resulting in DP-1 and DP-2 microstructures [32, 33].

The main focus of the present research work was to determine the reasons (both at micro level as well as nano level) as to why the dual phase microstructure of DP-2 steel with higher martensite content resulted in higher strength and also ductility as compared to DP-1 steel. For nano level investigations, nano-indentation tests were performed and for micro level investigations, spherical indentation tests were performed.

Thus, the main objective of the present research work was to **"analyze the effect of change in martensite volume fraction and grain size on tensile properties of DP steels using (i) tensile tests and also (ii) nano-indentation/spherical indentation techniques".**

The key issues taken up during the research work include:

- To subject the as-received steel through annealing routes of CAS-1 and CAS-2 in the Hot Dip Process Simulator (HDPS) to process DP-1 and DP-2 steels.
- To characterize the microstructures of DP-1 and DP-2 steels using scanning electron microscopy for evaluating martensite fraction and also grain size. Both, martensite volume fraction and grain size were determined using ImageJ software.
- Evaluation of mechanical properties of the two steels using tensile tests.
- Preparation of samples (before hardness tests) for flatness/surface finish using emery papers of different grades/polishing machine. Surface preparation of specimens is

important for spherical and nano-indentation hardness tests. For nano-indentation tests, specimens were also etched using 2% nital solution.

- Evaluation of nano-indentation hardness values across different layers (i.e. thickness) of DP-1 and DP-2 specimens to obtain contour plots. Contour plots presented in the research work provided hardness values for a given heat treated steel (DP-1/DP-2) for different combinations of load-depth of indentation-position. These hardness contour plots helped in evaluating the structure-tensile property relationship for DP-1 and DP-2 steels.
- Evaluation of spherical indentation hardness values across different layers (i.e. thickness) of DP-1 and DP-2 specimens. Hardness as a function of depth was plotted for both types of steel samples which helped in correlating results with nano-indentation data.

3.3 Experimental procedure for the present research work

The details pertaining to experimental procedure/methodology are as follows:

3.3.1 Starting material and processing

Steel sheets (0.83 mm finished thickness/67% cold rolled) of chemical composition as shown in Table 3.1 were used for experimental work. Steel samples of the starting material were subjected to two separate processing routes (CAS-1 and CAS-2; see Figure 3.1) as per the earlier reported work of [32, 33]. Hot Dip Process Simulator (HDPS) was used for annealing experiments. For heating of steel specimens, infra-red (IR) heating technique was used in gas mixture atmosphere of 'N_2+H_2' gases (with 10 vol. % H_2) to avoid oxidation of steel specimens during annealing in HDPS simulator. In the last step of annealing processes, specimens were ultra-fast cooled (cooling rate ~150 ℃/s) to room temperature by purging high pressure gas mixture. Thermocouples were spot welded to specimens to acquire the annealing temperature-time data.

3.3.2 Characterization and testing

A. ***Characterization using SEM and optical microscopy*****:** DP-1 and DP-2 steel specimens obtained as a result of annealing treatments were subjected to characterization using scanning electron microscopy (SEM) and optical microscopy. SEM micrographs and optical micrographs were obtained to identify the constituent phases, phase fraction, and grain size details for both DP-1 and DP-2 steel specimens.

B. ***Tensile testing of DP steels:*** DP-1 and DP-2 steels specimens were subjected to tensile testing to determine the ultimate tensile strength, yield strength, and percentage elongation of the two steels.

C. ***Nano-indentation hardness testing*****:** For nano-indentation testing, DP-1 and DP-2 steel samples were taken in the size of 10×10 (mm) as shown in Figure 3.2. Before nano-indentation testing, the steel specimens were prepared for adequate flatness/surface finish using emery papers of different grades and also polishing machine following the standard polishing procedures.

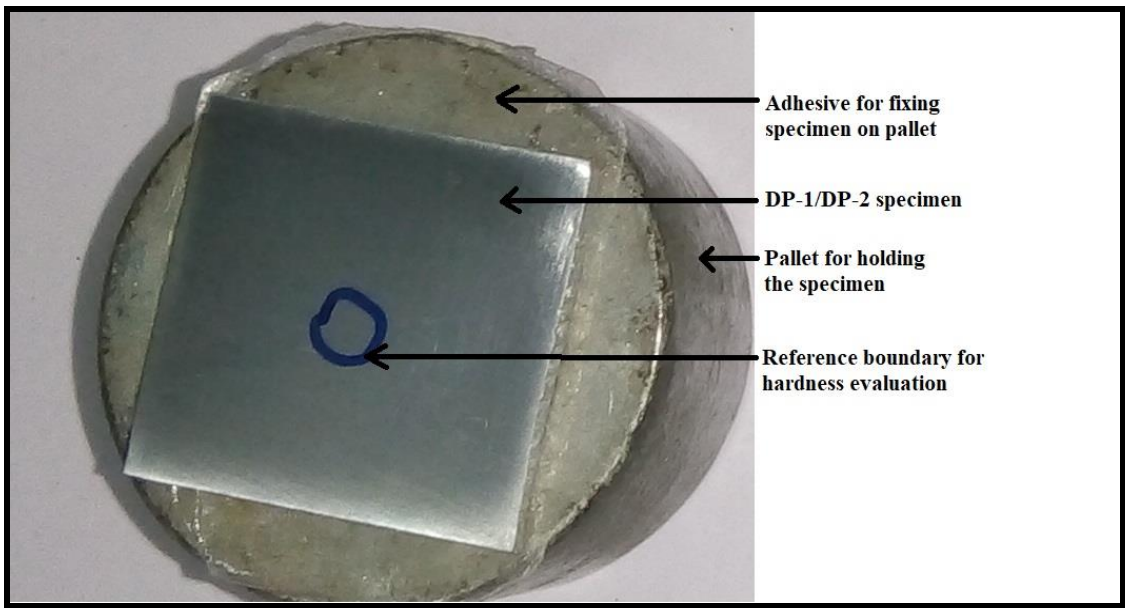

Figure 3.2 Steel specimen for nano-indentation hardness testing.

Nano-indentation hardness testing was carried out to in two different modes, (i) load mode, and (ii) depth of indentation mode, to cover the entire spectrum of load-depth of indentation regime during hardness testing.

(i) **Depth of indentation mode:** In the present work, for the nano-indentation testing in the 'depth of indentation' mode, progressive loading/un-loading was done till maximum depth of indentation of 3000 nm was obtained on the specimen during hardness testing. During progressive loading, the total number of un-loadings were kept as four. This mode covered the high load-high indentation conditions for hardness testing.

(ii) **Load mode:** In the present work, for the nano-indentation testing in the 'load' mode, a constant load of 0.5 mN was applied on the specimen during hardness testing. In this mode, there was single loading of low-constant load of 0.5 mN followed by un-loading,

followed by observation of depth of indentation. This mode covered the low load-low indentation conditions for hardness testing.

Figure 3.3 presents the schematic showing details of markings on DP-1/DP-2 specimen for nano-indentation hardness measurements.

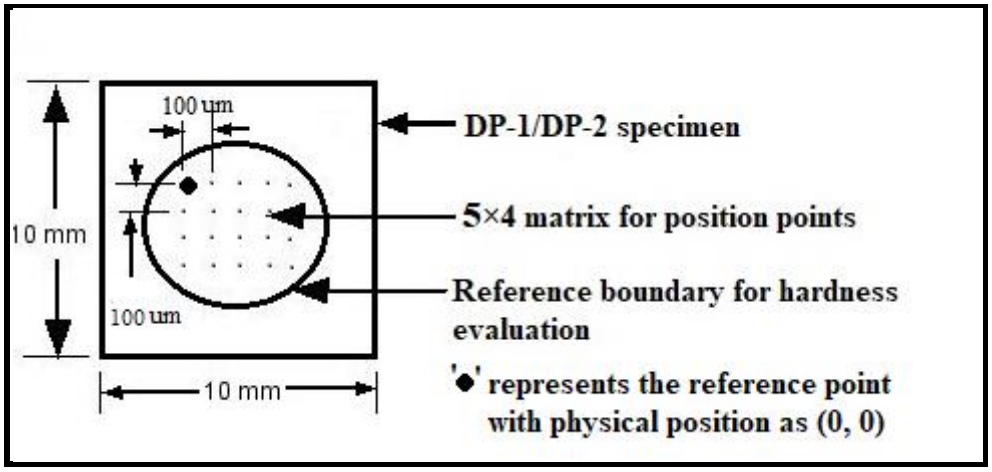

Figure 3.3 Schematic showing details of positions on specimen for nano-indentation hardness testing.

After completing the nano-indentation hardness testing for each mode, contour plots were plotted. Contour plots showed the variations in hardness as a function of various positions on the specimen, for each type of steel. Variation in hardness values at various positions on the specimen under a given loading condition were utilized to analyze the participation of phases present in microstructure of steel in the deformation process under loading.

Hardness (*H*) is measured in nano-indentation testing by the relation as shown in Equation 3.1.

$$\boldsymbol{H = \frac{P}{A}} \qquad \text{..... (3.1)}$$

Here, '*P*' is the load applied on the indenter and '*A*' is the projected area after indenter has penetrated into the sample. The projected area (*A*) depends on the depth indented in the sample and is given as Equation 3.2.

$$\boldsymbol{A = 24.5\ h_c^2} \qquad \text{..... (3.2)}$$

Here, 'h_c' is vertical distance along which the contact depth is made and is called contact depth. Further, modulus of elasticity (*E*) can be found by using the slope of un-loading curve 'S' which is expressed as Equation 3.3.

$$\mathbf{S = \frac{dP}{dh} = \frac{2E\sqrt{A}}{\sqrt{\pi}}} \qquad \text{..... (3.3)}$$

Also, 'E_r' is the reduced modulus and is expressed as Equation 3.4.

$$\frac{1}{E_r} = \frac{1-v^2}{E_r} + \frac{1-v_i^2}{E_i} \quad \text{..... (3.4)}$$

Here, E and *v* are the elastic modulus and Poisson's ratio of specimen material respectively. E_i and v_i are the elastic modulus and Poisson's ratio of the indenter material respectively. For diamond (i.e. indenter material), E_i = 1141 GPa and v_i = 0.07.

D. ***Spherical indentation hardness testing*:** Hardness measurement (Brinell hardness number, BHN) with the help of ball indentation (spherical indentation hardness testing) is expressed as shown in Equation 3.5. Spherical indentation tests were conducted in same manner as in nano-indentation (in depth of indentation mode). Difference was of scale on which measurement was done. In spherical indentation testing in the present work, maximum load of approximately 1200 N was applied and corresponding maximum depth was 0.73 mm. Hardness measurements were done under progressive loading on each specimen. During progressive loading, the total number of loadings/un-loadings were kept as eight. Unlike, depth of indentation mode, where 20 different positions were analysed on each sample, in spherical indentation, only two positions were analyzed for hardness testing.

$$\mathbf{BHN} = \frac{\mathbf{2P}}{\left[\pi.\mathbf{D}\left(\mathbf{D}-\sqrt{\left(\mathbf{D^2}-\mathbf{d_t^2}\right)}\right)\right]} \quad \text{..... (3.5)}$$

Here, 'P' is the load applied, 'D' is the diameter of the spherical ball indenter (in present work, indenter diameter was 1.5 mm), 'd_t' is the diameter of indentation impression formed on the specimen surface. In the present work, 'd_t' was measured using ImageJ software.

3.4 Machines and equipment

3.4.1 Hot dip process simulator (HDPS)

HDPS set-up (Make: ICS Surtec Research Corporation, UK) was used for annealing simulations for processing DP-1 and DP-2 steel specimens (see Figure 3.4). This is a highly automated machine which can be used for galvanizing and annealing of sheet metal specimens. HDPS set-up uses infrared heating system. The maximum achievable annealing temperature, heating rate, and cooling rate values with this set-up are 1200 ℃, 30 ℃/s, and 150 ℃/s respectively. The specimen to be heat treated in HDPS set-up is mounted on the end of a rod,

which is operated by an automatic system. The rod moves in/out of the heating and cooling chambers according to requirements of annealing cycle. Thermocouple is directly spot welded on the specimens to get accurate temperature values. In the present work, a mixture of H_2 (10 vol. %) and N_2 (90 vol. %) gases was used to create an inert atmosphere to prevent oxidation of specimens during heat treatment. The required annealing parameters are fed directly to the machine input device.

Figure 3.4 Hot dip process simulator [Courtesy: CSIR-NML, Jamshedpur].

3.4.2 Tensile testing machine

Tensile tests were conducted on a tensile testing machine (Make: Instron 8862 System, Instron Engineering Corporation, USA) of 100 kN load capacity at room temperature. Figure 3.5 shows the set-up. Dog bone shaped tensile samples as per ASTM standard E-8M were used for testing.

Figure 3.5 Tensile testing machine [Courtesy: CSIR-NML, Jamshedpur].

3.4.3 Grinding, polishing and etching

DP-1/DP-2 specimens were subjected to grinding/polishing before nano-indentation testing. Finishing has a significant effect on nano-indentation testing as rough surfaces give inaccurate and undesirable results as indenter might project on a rough peak.

The specimens were initially grinded using emery papers of various grades (see Figure 3.6). The abrasive papers used included grades of 80, 120, 220, 400, 600, 800, and 1000. Care was taken to apply the correct pressure using emery papers as high pressure puts scratches on the specimen surface. Also, direction of polishing was taken care of. Initially, the specimen was polished horizontally and subsequently vertically. The same alternate sequence was used while using emery papers of each grade.

Figure 3.6 Abrasive papers of various grades used in the present research.

Next, polishing machine (Make: Banipol METCO, Model No: PMV018, Chennai Metco Private Limited, India) as shown in Figure 3.7 was used to polish DP-1/DP-2 specimens against a rotating disk on which a soft cloth (velvet/canvas) was attached. The specimen surface was rubbed against the cloth in presence of alumina colloidal solution.

Figure 3.7 Polishing machine [Courtesy: CSIR-NML, Jamshedpur].

After polishing, the specimen surface was etched chemically. Etching was done in order to clearly see the microstructure of specimens under the microscope. Nital (2 % nitric acid mixed in ethanol) was applied on the specimen surface for 10–20 s and then washed away with water.

3.4.4 Scanning electron microscope

FE-SEM set-up (Make: Nova Nano SEM 430; Field Electron and Ion Company, USA) was used to obtain SEM micrographs of DP-1/DP-2 steel specimens for observing the dual phase

microstructures. These micrographs were used to determine phase fraction of constituent phases and martensite grain size in each steel. Figure 3.8 shows the FE-SEM set-up used in the present work.

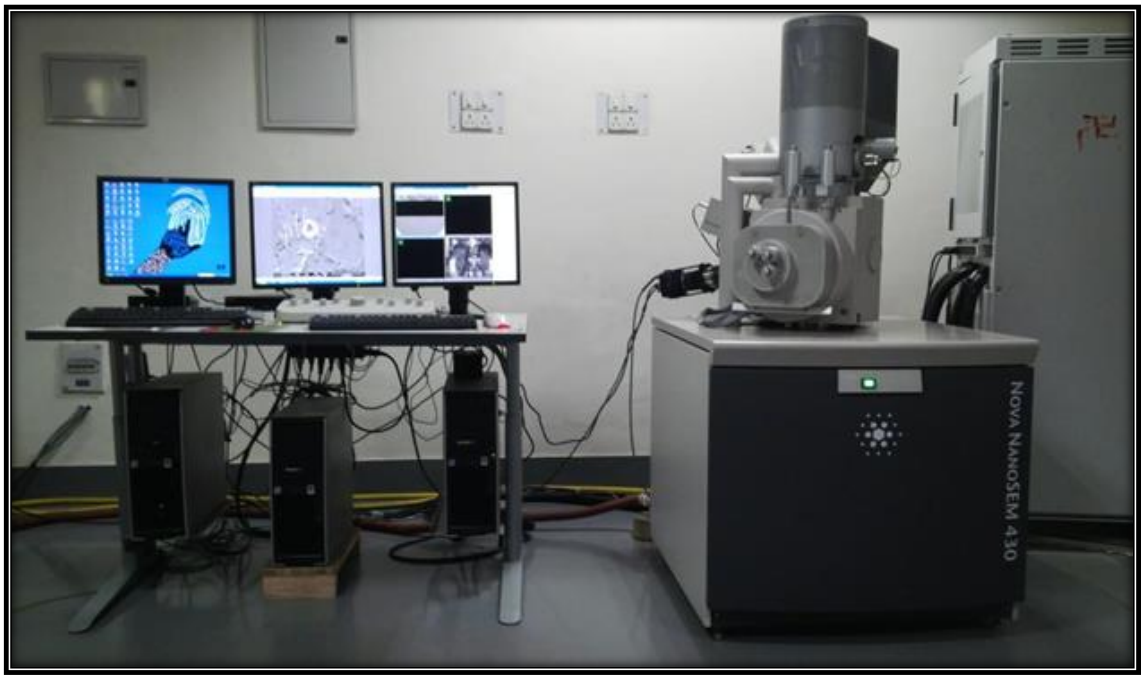

Figure 3.8 Scanning electron microscope [Courtesy: CSIR-NML, Jamshedpur].

3.4.5 Nano-indentation machine

The nano-indentation set-up (Make: MTS Nano-Indenter XP, USA) performs indentation tests by driving the indenter into surface of specimen and collects applied load and depth of indentation data. These data values are used to determine material properties (mainly hardness and modulus of elasticity). In the present work, nano-indentation tests were done on this set-up to evaluate variation in hardness as a function of depth of indentation under various loading/un-loading conditions. Nano-indentation machine used in the present work is shown in Figure 3.9. The maximum applied load and maximum depth of indentation values for the set-up are 500 mN and 500 µm respectively. Specimens for hardness testing are mounted (by glue) on a standard cylinder (31.75 mm in diameter). Diamond indenter (Berkovich type) with a standard cone angle of 72.32° was used.

Figure 3.9 Nano-indentation machine [Courtesy: CSIR-NML, Jamshedpur].

3.4.6 Spherical indentation machine

Automated macro indentation tester (AMIT) or spherical indentation machine (Make: DUCOM Instruments, India) determines the load-displacement data of a ball indenter during loading/un-loading of specimens during testing. This data is used to determine material properties (like hardness, yield strength, ultimate tensile strength, elastic modulus etc.). In the present work, spherical indentation tests were done on this set-up to evaluate variation in hardness as a function of depth of indentation under various loading/un-loading conditions. Spherical indentation machine used in the present work is shown in Figure 3.10. The maximum applied load and maximum depth of indentation values for the set-up are 3.5 kN and 2.0 mm respectively. Specimens for hardness testing are mounted (by glue) on a standard cylinder (31.75 mm in diameter). Diamond ball indenter of size 1.5 mm was used in the present research.

Figure 3.10 Spherical indentation machine [Courtesy: CSIR-NML, Jamshedpur].

3.4.7 Leveling

To find the diameter of indentation impression of spherical ball in the spherical indentation test, optical microscope is needed. However, for optical imaging, the specimen surface must be completely flat. Leveling machine (Figure 3.11) was used to lay the specimen surface in flat orientation. For this, after the spherical indentation test, the DP-1/DP-2 specimen was taken for leveling. The circular plate attached to the leveling machine pressed the specimen against a soft material like clay. Precautions were taken that while pressing the plate directly over the specimen surface, the surface does not get scratches. To avoid this problem, tissue paper was kept over the specimen surface and now circular plate was pressed with normal force.

Figure 3.11 Leveling machine [Courtesy: CSIR-NML, Jamshedpur].

3.4.8 Optical microscope

Optical microscope (Make: Leica DM2500M; *Leica Microsystems*, Wetzlar, Germany) as shown in Figure 3.12 was used in the present work to measure the diameter of indentation impression formed on the specimen surface during spherical indentation testing.

Figure 3.12 Optical microscope [Courtesy: CSIR-NML, Jamshedpur].

3.4 Commercial Software

The details of various software used in the present study are describes as follows:

3.5.1 Origin

Origin is a commercial software developed by OriginLab Corporation, US and mainly used for statistics, curve fitting etc. In the present work, Origin software was used for making contour plots from nano-indentation data. Also, other plots like hardness versus depth, load versus depth were also plotted using this software.

3.5.2 ImageJ

ImageJ is open source software mainly used for image analysis. ImageJ is developed by National Institute of Health, US. In the present study, ImageJ software was used for determination of phase fraction/grain size in dual phase microstructures of DP-1/DP-2 steels specimens. Further, it was used to determine the diameter of indentation impression obtained during spherical indentation test.

CHAPTER 4
RESULTS AND DISCUSSION

4.1 General

This chapter discusses the main results obtained in the present experimental work. Two different core and shell type dual phase microstructures (DP-1 and DP-2) were obtained in the starting material through variations in heat treatment route. Tensile properties of DP-1 and DP-2 steels were determined and reasons for difference in their properties were explored from microstructure viewpoint. However, the main focus of this dissertation work was to explain the difference in tensile properties of DP-1 and DP-2 steels from their hardness distribution. Two main hardness tests viz. nano-indentation test and spherical indentation test were conducted.

4.2 Microstructure of DP-1 and DP-2 steels

Figure 4.1a–b presents the microstructure of DP-1 and DP-2 steels. Both the dual phase microstructures (containing ferrite and martensite phases) were typical core and shell type microstructures containing martensite as the core surrounded by ferrite channel network as the shell. Martensite volume fraction (MVF) in the microstructure of DP-1 and DP-2 steels was determined using ImageJ software as 52.2% and 62.2% respectively. Further, grain size of martensite was determined using ImageJ. Martensite grain size was relatively finer in DP-2 steel. Martensite grain size was determined as 4.63 μm and 3.09 μm for DP-1 and DP-2 steels respectively.

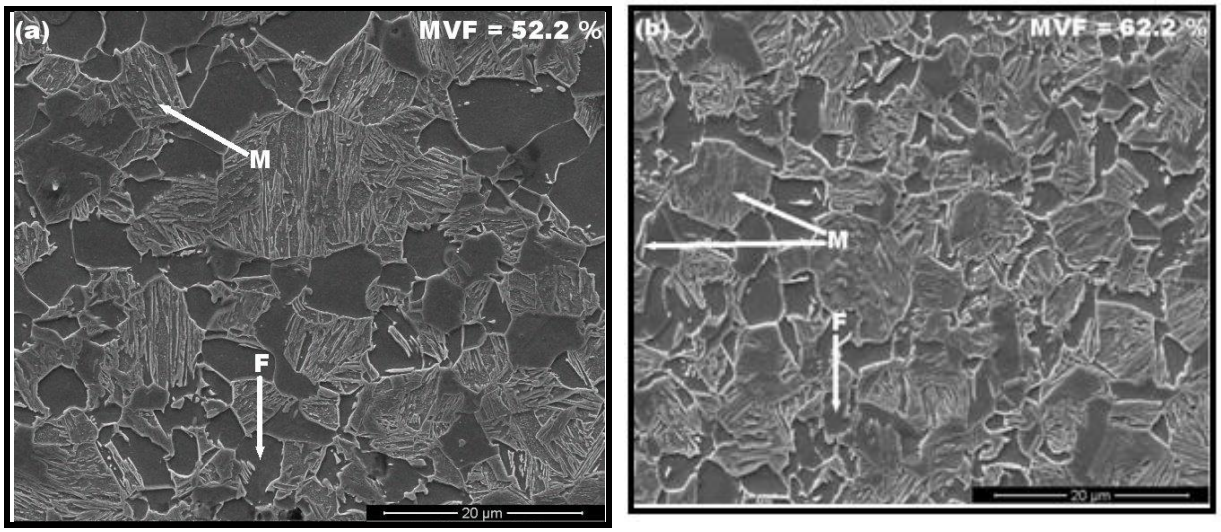

Figure 4.1 SEM micrographs showing microstructure of (a) DP-1 steel, and (b) DP-2 steel.

4.3 Tensile properties of DP-1 and DP-2 steels

The tensile properties obtained in DP-1 and DP-2 steels are presented in Table 4.1 along with details of martensite fraction and grain size.

Table 4. 1 Tensile properties of DP-1 and DP-2 steels.

Type of steel with DP microstructure obtained after heat treatment	Martensite volume fraction, MVF (%)	Martensite grain size (μm)	Ultimate tensile strength, UTM (MPa)	Yield strength, YS (MPa)	Uniform elongation, UE (%)
DP-1	52.2	4.63	980	570	11
DP-2	62.2	3.09	1054	637	12

The engineering stress-strain curve for DP-1 and DP-2 steels is presented in Figure 4.2. It can be observed that DP-2 steel containing relatively larger martensite volume fraction with finer martensite grain size provided better strength values and also comparable ductility.

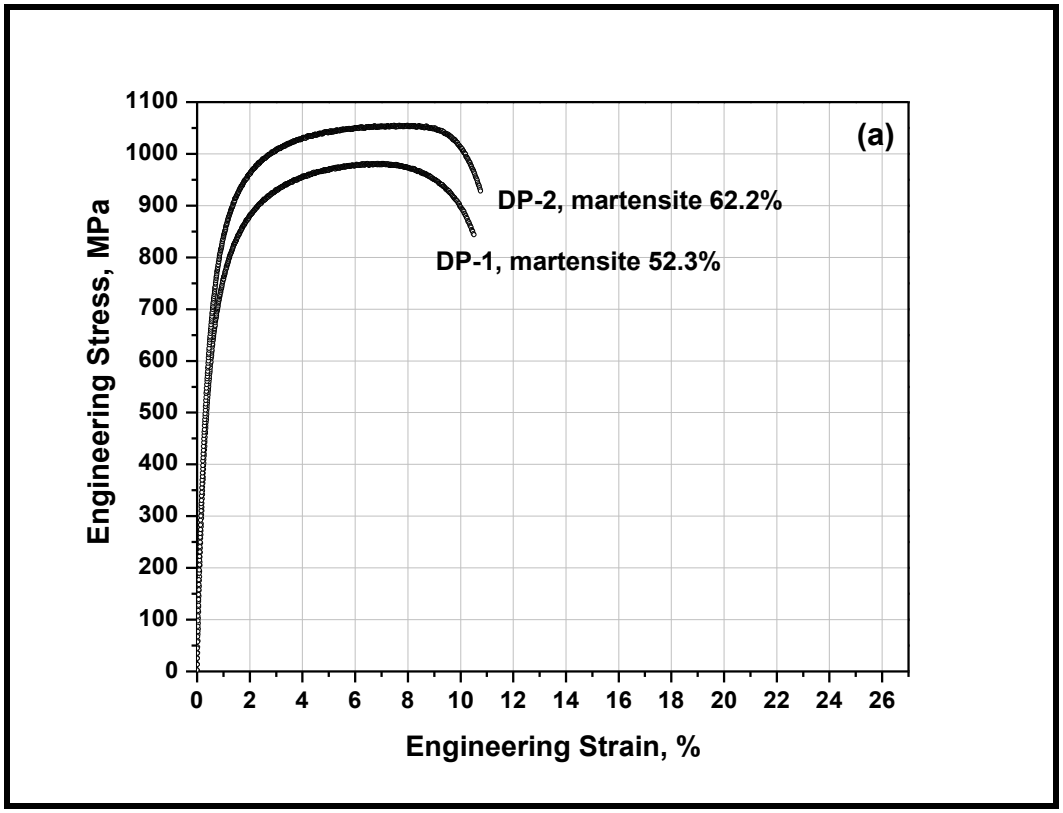

Figure 4.2 Stress-strain curves of DP-1 and DP-2 steels.

Though CAL process (‘continuous annealing line’ process) is the industrially accepted route for processing of dual phase steels, but better annealing routes are being researched to improve the mechanical properties of DP steels, especially the strength-ductility combination. One of

the novel annealing routes in this research area is the core and shell (or harmonic) type dual phase microstructure with hard phase surrounded by the softer phase (i.e. martensite in the core and ferrite in the shell). In the present work, DP-1 and DP-2 steels, both contained core and shell type DP microstructure with difference in martensite fraction and grain size. DP-2 with larger martensite fraction and finer grain sized showed better strength-ductility combination. It is well reported in literature that mechanical properties of DP steels depend on grain size of ferrite phase, and on volume fraction, carbon content, morphology, and distribution of martensite phase present in the ferrite matrix of the dual phase microstructure. Authors have reported that larger martensite fraction increases the yield strength as well as ultimate tensile strength [21]. Erdogan *et al* [35] investigated the influence of martensite size distribution on properties of DP steels. Yield strength and ultimate tensile strength increased with fine martensite distribution in ferrite matrix. Finer martensite provided more restriction to dislocation movement and greater strengthening for the same martensite content. Thus, in the present work, DP-2 steel with higher martensite fraction/finer grain size showed superior strength values. Further, researchers have reported that ductility of DP steels is largely affected by morphology and grain size of martensite phase. The fine fibrous/globular type martensite results in higher total elongation compared to coarser/blocky type martensite Also, Kumar *et al.* [33] reported that in core and shell type DP microstructure, the ferrite channel present at the inter-martensite grain regions retards the crack growth rate and prevents the cracks from entering into adjacent martensite regions. This phenomenon delays the onset of global deformation and hence increases the ductility of DP steels. Similarly, Singh *et al.* [32] showed that during tensile deformation of DP steels with CAS type microstructure, the micro-cracks generated in martensite phase get blunt/dampened because of the presence of the surrounding soft/ductile ferrite phase. In the light of this, DP-2 steel with relatively finer martensite grain size displays better resistance to crack growth or better dampening of micro-cracks generated in the martensite phase, and thus shows slightly superior ductility as compared to DP-1 steel.

4.4 Nano-indentation hardness results

This section describes the results of nano-indentation hardness testing.

4.4.1 Nano-indentation hardness testing in depth mode

Table 4.2 and Table 4.3 present the results of nano-indentation hardness testing of DP-1 and DP-2 steels respectively conducted in the depth mode.

Table 4.2 Nano-indentation hardness values in depth mode with regards to various layers for DP-1 steel.

Physical position w.r.t to reference point (µm)	Matrix position (m×n)	Layer number (Unloading number)	Load, P (mN)	Depth of indentation, h_c (nm)	Hardness (GPa)	Physical position w.r.t to reference point (µm)	Matrix position (m×n)	Layer number (Unloading number)	Load, P (mN)	Depth of indentation, h_c (nm)	Hardness (GPa)
FIRST ROW OF THE 5×4 MATRIX (DP-1 STEEL)						***SECOND ROW OF THE 5×4 MATRIX (DP-1 STEEL)***					
(0, 0)	1×1	1	60.71	1007.23	2.58	(100, 0)	2×1	1	60.55	1059.06	2.29
		2	121.96	1450.22	2.49			2	121.52	1564.11	2.09
		3	243.57	2036.87	2.53			3	242.38	2139.09	2.25
		4	490.58	2831.34	2.47			4	489.90	2842.01	2.60
(0, 100)	1×2	1	60.57	1023.66	2.49	(100, 100)	2×2	1	61.28	1014.14	2.56
		2	121.47	144.27	2.52			2	121.21	1411.95	2.62
		3	242.35	1975.52	2.69			3	245.00	1970.82	2.73
		4	489.62	2814.36	2.68			4	488.46	2724.56	2.86
(0, 200)	1×3	1	60.55	873.22	3.4	(100, 200)	2×3	1	60.55	1066.89	2.25
		2	121.32	1209.91	3.58			2	121.36	1469.69	2.41
		3	242.18	1695.39	3.67			3	242.23	2031.53	2.51
		4	488.92	2427.77	3.63			4	488.83	2827.33	2.63
(0, 300)	1×4	1	61.02	919.47	3.15	(100, 300)	2×4	1	60.69	944.84	2.95
		2	122.52	1286.63	3.23			2	121.31	1376.97	2.76
		3	244.37	1886.06	3.0			3	241.9	1885.97	2.95
		4	487.15	2661.29	2.99			4	488.59	2660.77	3.01
(0, 400)	1×5	1	61.21	1059.18	3.15	(100, 400)	2×5	1	60.55	1058.56	2.29
		2	122.61	1377.17	3.23			2	121.31	1466.75	2.40
		3	244.76	1863.92	3.00			3	242.48	2013.04	2.56
		4	487.52	2558.17	2.99			4	489.89	2734.26	2.83

Physical position w.r.t to reference point (μm)	**Matrix position (m×n)**	**Layer number (Unloading number)**	**Load, P (mN)**	**Depth of indentation, h_c (nm)**	**Hardness (GPa)**	**Physical position w.r.t to reference point (μm)**	**Matrix position (m×n)**	**Layer number (Unloading number)**	**Load, P (mN)**	**Depth of indentation, h_c (nm)**	**Hardness (GPa)**
THIRD ROW OF THE 5×4 MATRIX (DP-1 STEEL)						***FOURTH ROW OF THE 5×4 MATRIX (DP-1 STEEL)***					
(200, 0)	3×1	1	60.57	845.99	3.65	(300, 0)	4×1	1	60.55	984.99	2.66
		2	121.82	1195.05	3.67			2	121.01	1369.52	2.76
		3	243.09	1623.02	4.12			3	244.82	1912.68	2.88
		4	484.50	2277.95	4.03			4	487.34	2614.69	3.09
(200, 100)	3×2	1	61.25	991.45	2.66	(300, 100)	4×2	1	61	1109.51	2.1
		2	121.19	1360.66	2.80			2	122.21	1501.55	2.30
		3	244.97	1858.31	3.06			3	243.74	2040.72	2.51
		4	488.33	2574.96	3.19			4	485.95	2783.79	2.71
(200, 200)	3×3	1	60.54	1132.05	2	(300, 200)	4×3	1	60.74	859.41	3.54
		2	121.23	1599.02	2.02			2	122.91	1245.89	3.42
		3	243.40	2182.38	2.18			3	243.71	1804.66	3.23
		4	484.81	2942.65	2.40			4	485.84	2509.44	3.35
(200, 300)	3×4	1	61.19	921.98	3.11	(300, 300)	4×4	1	60.84	868.14	3.51
		2	122.57	1379.00	2.77			2	121.96	1325.19	2.99
		3	243.07	2003.04	2.60			3	243.45	1886.69	2.95
		4	484.68	2779.05	2.71			4	484.92	2608.27	3.09
(200, 400)	3×5	1	60.75	1194.55	1.79	(300, 400)	4×5	1	60.84	940.93	2.98
		2	121.82	1584.67	2.06			2	121.94	1284.36	3.22
		3	243.04	2112.08	2.33			3	243.45	1807.71	3.26
		4	484.49	2851.88	2.56			4	484.62	2595.73	3.15

Table 4.3 Nano-indentation hardness values in depth mode with regards to various layers for DP-2 steel.

Physical position w.r.t to reference point (μm)	*Matrix position (m×n)*	*Layer number (Unloading number)*	*Load, P (mN)*	*Depth of indentation, h_c (nm)*	*Hardness (GPa)*	*Physical position w.r.t to reference point (μm)*	*Matrix position (m×n)*	*Layer number (Unloading number)*	*Load, P (mN)*	*Depth of indentation, h_c (nm)*	*Hardness (GPa)*
FIRST ROW OF THE 5×4 MATRIX (DP-2 STEEL)						***SECOND ROW OF THE 5×4 MATRIX (DP-2 STEEL)***					
(0, 0)	1×1	1	60.60	1269.18	1.57	(100, 0)	2×1	1	61.15	1006.19	2.56
		2	121.54	1691.15	1.78			2	122.58	1361.34	2.82
		3	243.36	2298.45	1.94			3	245.38	1899.96	2.91
		4	486.81	3058.82	2.20			4	488.2	2701.5	2.88
(0, 100)	1×2	1	60.54	1000.51	2.57	(100, 100)	2×2	1	60.69	1114.89	2.06
		2	122.86	1468.08	2.40			2	121.62	1558.03	2.11
		3	243.09	2241.35	2.05			3	243.78	2145.38	2.24
		4	489.69	3146.5	2.09			4	484.63	2869.62	2.51
(0, 200)	1×3	1	61	927.4	3.02	(100, 200)	2×3	1	60.56	893.48	3.23
		2	122.24	1337.61	2.94			2	121.34	1204.96	3.59
		3	244.71	1914.96	2.86			3	243.16	1683.05	3.7
		4	489.13	2786.45	2.69			4	489.87	2513.0	3.35
(0, 300)	1×4	1	60.89	1178.72	1.83	(100, 300)	2×4	1	60.71	813.36	3.97
		2	121.99	1545.18	2.14			2	121.65	1182.05	3.78
		3	244.58	2091.11	2.38			3	243.87	1756.65	3.42
		4	489.41	2944.67	2.40			4	484.67	2603.09	3.1
(0, 400)	1×5	1	60.79	1140.11	1.96	(100, 400)	2×5	1	60.58	1334.03	1.41
		2	121.88	1563.65	2.11			2	121.05	1690.47	1.77
		3	244.10	2135.75	2.27			3	242.55	2172.23	2.17
		4	485.85	2878.08	2.49			4	488.66	2936.52	2.41

Physical position w.r.t to reference point (μm)	*Matrix position (m×n)*	*Layer number (Unloading number)*	*Load, P (mN)*	*Depth of indentation, h_c (nm)*	*Hardness (GPa)*	*Physical position w.r.t to reference point (μm)*	*Matrix position (m×n)*	*Layer number (Unloading number)*	*Load, P (mN)*	*Depth of indentation, h_c (nm)*	*Hardness (GPa)*
THIRD ROW OF THE 5×4 MATRIX (DP-2 STEEL)						***FOURTH ROW OF THE 5×4 MATRIX (DP-2 STEEL)***					
(200, 0)	3×1	1	60.95	1083.29	2.2	(300, 0)	4×1	1	60.75	968.79	2.76
		2	122.22	1473.75	2.39			2	122.16	1361.38	2.81
		3	244.68	2049.88	2.48			3	244.62	1892.2	2.92
		4	489.70	2833.90	2.60			4	489.40	2698.59	2.89
(200, 100)	3×2	1	60.62	892.03	3.27	(300, 100)	4×2	1	60.63	868.82	3.46
		2	121.59	1284.06	3.17			2	121.55	1280.61	3.18
		3	243.37	1846.74	3.06			3	243.13	1890.19	2.92
		4	484.2	2631.90	3.01			4	490.16	2802.68	2.67
(200, 200)	3×3	1	60.53	1167.7	1.86	(300, 200)	4×3	1	60.54	783.99	4.30
		2	121.30	1567.97	2.08			2	121.31	1177.02	3.7
		3	243.13	2073.08	2.41			3	243.12	1758.81	3.38
		4	489.96	2867.98	2.55			4	489.82	2632.61	3.03
(200, 300)	3×4	1	60.53	1095.53	2.14	(300, 300)	4×4	1	60.55	1211.09	1.74
		2	121.31	1526.01	2.22			2	121.33	1614.73	1.96
		3	243.14	2045.90	2.47			3	243.09	2195.42	2.14
		4	489.54	2854.88	2.57			4	490.22	3038.1	2.26
(200, 400)	3×5	1	60.72	1328.14	1.43	(300, 400)	4×5	1	61.24	989.27	2.66
		2	121.65	1771.21	1.62			2	122.74	1371.69	2.79
		3	243.79	2365.09	1.83			3	242.66	1971.22	2.66
		4	484.68	3105.6	2.12			4	485.77	2800.54	2.65

Figure 4.3 (as shown below) presents the contour plots showing hardness distribution in the two steels (DP-1 and DP-2) under different test conditions (depth mode) shown in Table 4.2 and Table 4.3.

DP-1 STEEL, LAYER 1	DP-2 STEEL, LAYER 1
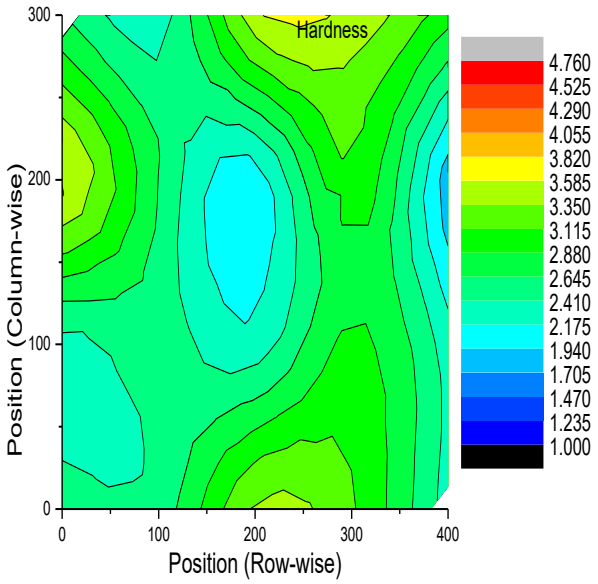	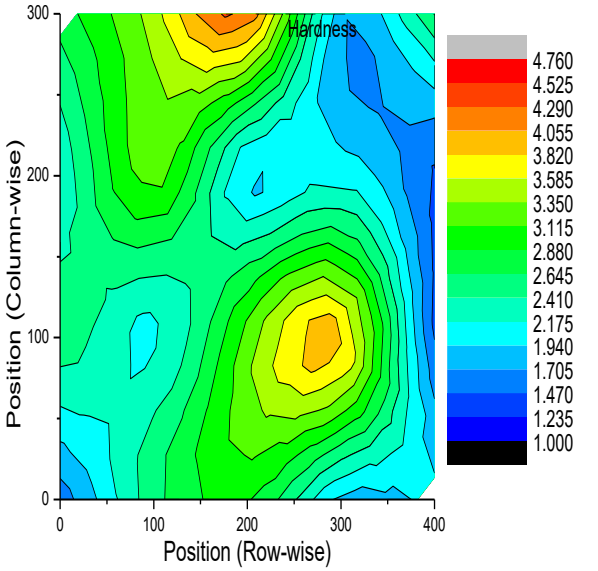
DP-1 STEEL, LAYER 2	**DP-2 STEEL, LAYER 2**
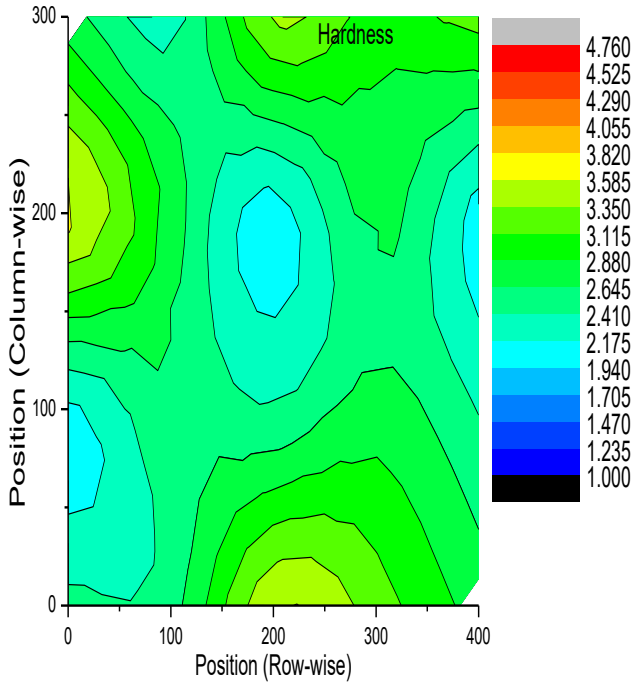	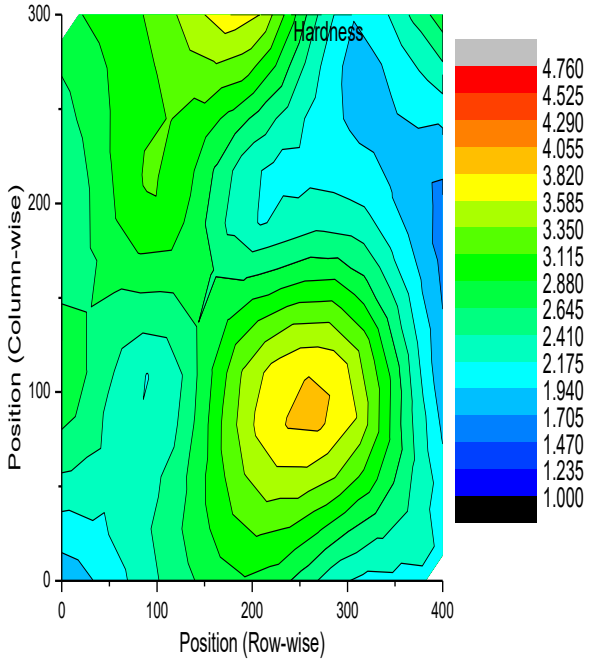
DP-1 STEEL, LAYER 3	**DP-2 STEEL, LAYER 3**

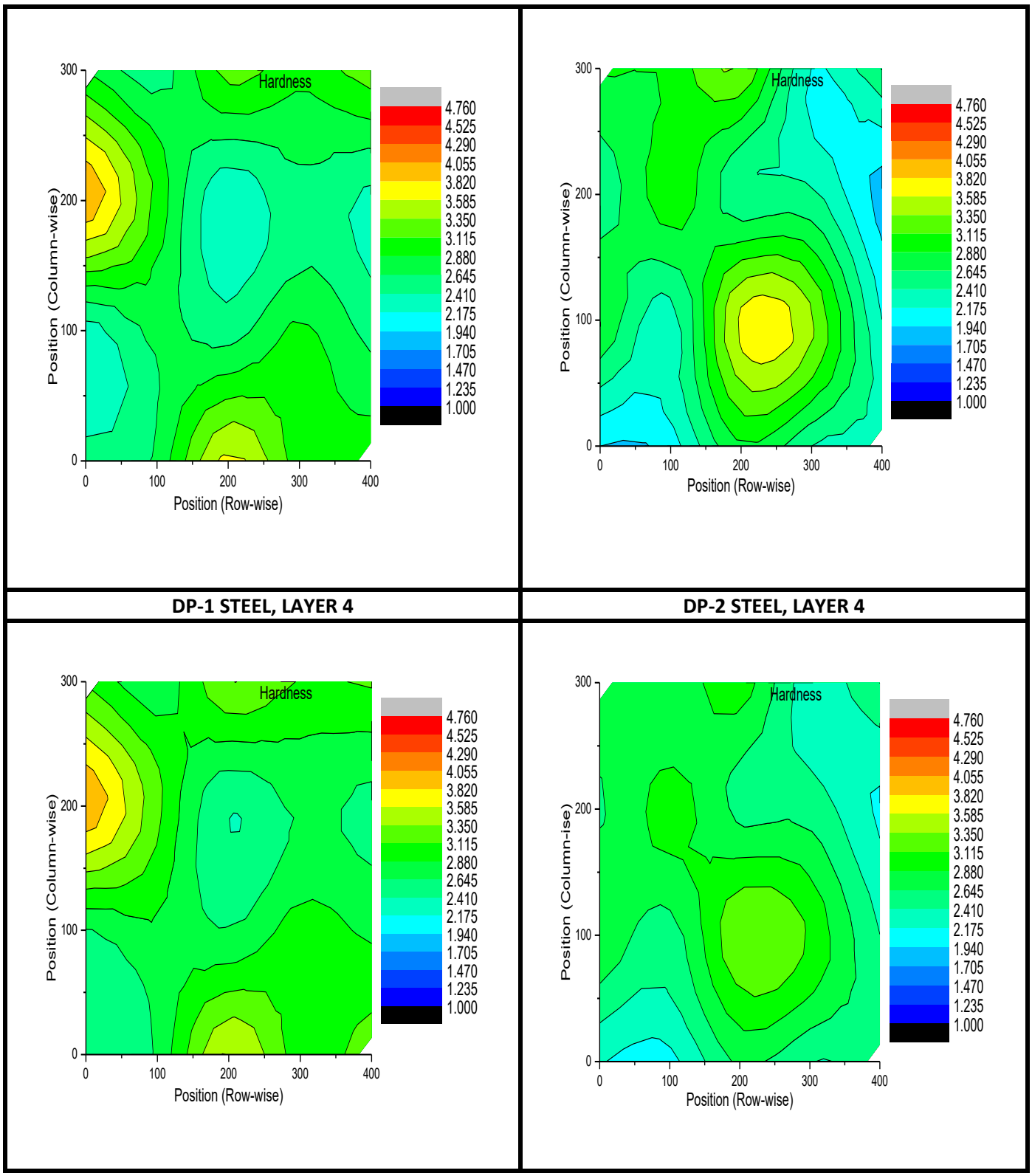

Figure 4.3 Contour plots showing variations in nano-indentation hardness values in depth mode with regards to various layers for DP-1 and DP-2 steels.

Contour plots (Figure 4.3) are representing the hardness distribution in the marked area (i.e. the area under investigation as shown in Figure 3.2 and Figure 3.3) for various layers of DP-1

and DP-2 steels. Specimens were subjected to progressive loading (0–450 mN) to attain a maximum depth of indentation of 3000 nm in both the steels. During this progressive loading, specimens were unloaded for a total of 4 times. Each case of un-loading was considered as a layer, and the data pertaining to load applied, depth of indentation, and hardness value was determined for all the points (the 20 physical positions in the marked area) on DP-1/DP-2 specimens. This procedure was followed and nano-indentation hardness data as is presented in Table 4.3 and 4.4 was collected to plot the contour plots.

For the marked area under investigation, contour plots are actually representing the manner in which micro structural constituents are participating in resisting indentation under load during nano-hardness testing. In other words, contour plots are representing the participation (or contribution) of micro-constituents of ferrite and martensite (of DP microstructure) in the deformation process during nano-indentation hardness testing (and so also during tensile testing). Further, it may be noted that under a given loading condition (i.e. at a given layer), if the contour plot is showing even distribution of hardness at all places (i.e. if there are too less variations in color across the plot), it is only one of the phases of the DP microstructure that is largely participating in the deformation process. On the contrary, if contour plot is showing variations in hardness at different places (i.e. if there are variations in color across the plot), it is both the phases of the DP microstructure that are participating in the deformation process.

In the present work, for Layer 1 of DP-1 steel, the contour plot (see Figure 4.3) showed more even distribution of hardness throughout the marked area. This signified that for DP-1 steel, only one of the two phases of the DP microstructure was largely/significantly participating in the deformation process. However, for Layer 1 of DP-2 steel, the contour plot (Figure 4.3) was quite different with significant variations in hardness throughout the marked area (changes in colour throughout the plot). This signified that for DP-2 steel, both the constituent phases participated actively in the deformation process (e.g. the large volume fraction of blue region reflects presence of lower hardness phase of microstructure i.e. ferrite participation in deformation). Further, comparison of Layer 2, Layer 3, and Layer 4 for DP-1 and DP-2 steels also showed similar results. (it was noted by comparing all the layers [Layer 1–Layer 4] for the two steels that for DP-1 steel, the low hardness blue region was almost absent, whereas DP-2 steel was displaying the entire spectrum of hardness values ranging from the minimum hardness represented by dark blue colour to the maximum hardness by (Represent secondary phase of microstructure around the primary phase or finer grain size of constituent phases, or both. From these observations, it was concluded that because of the participation of both the

constituent phases in the deformation process, DP-2 steel provided better strength and ductility as compared to DP-1 steel.

4.4.2 Nano-indentation hardness testing in load mode

Nano-indentation hardness testing was carried out at a constant low load of 0.5 mN to investigate the hardness distribution in the two steels even under low depths of indentation. Table 4.4 and Table 4.5 present the results of nano-indentation hardness testing of DP-1 and DP-2 steels respectively conducted in the load mode.

Figure 4.4 (as shown below) presents the contour plots showing hardness distribution in the two steels (DP-1 and DP-2) under different test conditions (load mode) shown in Table 4.4.

Contour plots (Figure 4.4) are representing the hardness distribution in the marked area (i.e. the area under investigation as shown in Figure 3.2 and Figure 3.3) for DP-1 and DP-2 steels. Specimens were subjected to a constant low load of 0.5 mN. Unlike depth mode (where load was not constant but was progressive with specimens being unloaded several times), in the load mode, the specimen was unloaded just once, after application of constant low load of 0.5 mN. On unloading, the data pertaining to depth of indentation and hardness value was determined for all the points (the 20 physical positions in the marked area) on DP-1/DP-2 specimens. This procedure was followed and nano-indentation hardness data as is presented in Table 4.4 was collected to plot the contour plots.

Table 4.4 Nano-indentation hardness values in load mode for DP-1 and DP-2.

Physical position w.r.t to reference point (μm)	Matrix position (m×n)	Layer number (Unloading number)	Load, P (mN)	Depth of indentation, h_c (nm)	Hardness (GPa)	Physical position w.r.t to reference point (μm)	Matrix position (m×n)	Layer number (Unloading number)	Load, P (mN)	Depth of indentation, h_c (nm)	Hardness (GPa)
HARDNESS DATA FOR DP-1 STEEL											
FIRST ROW OF THE 5×4 MATRIX (DP-1 STEEL)						***SECOND ROW OF THE 5×4 MATRIX (DP-1 STEEL)***					
(0, 0)	1×1		0.49	194.84	0.52	(100, 0)	2×1		0.49	59.05	5.78
(0, 100)	1×2		0.49	101.09	2.01	(100, 100)	2×2		0.49	157.95	0.78
(0, 200)	1×3	---	0.49	85.19	2.75	(100, 200)	2×3	---	0.49	129.91	1.18
(0, 300)	1×4		0.49	427.05	0.106	(100, 300)	2×4		0.49	144.91	0.96
(0, 400)	1×5		0.49	89.81	2.45	(100, 400)	2×5		0.49	257.22	0.30
THIRD ROW OF THE 5×4 MATRIX (DP-1 STEEL)						***FOURTH ROW OF THE 5×4 MATRIX (DP-1 STEEL)***					
(200, 0)	3×1		0.49	80.55	3.11	(300, 0)	4×1		0.49	242.64	0.33
(200, 100)	3×2		0.49	146.37	0.95	(300, 100)	4×2		0.49	95.69	2.10
(200, 200)	3×3	---	0.49	66.16	5.15	(300, 200)	4×3	---	0.49	249.51	0.32
(200, 300)	3×4		0.49	118.62	1.39	(300, 300)	4×4		0.49	254.66	0.29
(200, 400)	3×5		0.49	90.72	2.47	(300, 400)	4×5		0.49	48.65	8.48
HARDNESS DATA FOR DP-2 STEEL											
FIRST ROW OF THE 5×4 MATRIX (DP-2 STEEL)						***SECOND ROW OF THE 5×4 MATRIX (DP-2 STEEL)***					
(0, 0)	1×1		0.49	76.36	3.43	(100, 0)	2×1		0.49	74.98	3.54
(0, 100)	1×2		0.49	95.51	2.23	(100, 100)	2×2		0.49	154.22	0.81
(0, 200)	1×3	---	0.49	78.47	3.25	(100, 200)	2×3	---	0.49	178.23	0.63
(0, 300)	1×4		0.49	195.00	0.53	(100, 300)	2×4		0.49	64.97	4.95
(0, 400)	1×5		0.49	113.92	1.57	(100, 400)	2×5		0.49	58.48	6.0
THIRD ROW OF THE 5×4 MATRIX (DP-2 STEEL)						***FOURTH ROW OF THE 5×4 MATRIX (DP-2 STEEL)***					
(200, 0)	3×1		0.49	58.47	1.39	(300, 0)	4×1		0.49	120.16	1.3
(200, 100)	3×2		0.49	121.49	9.67	(300, 100)	4×2		0.49	104.08	1.82
(200, 200)	3×3	---	0.49	47.56	2.8	(300, 200)	4×3	---	0.49	153.00	0.86
(200, 300)	3×4		0.49	85.39	4.53	(300, 300)	4×4		0.49	118.52	1.46
(200, 400)	3×5		0.49	67.02	5.2	(300, 400)	4×5		0.49	61.83	5.42

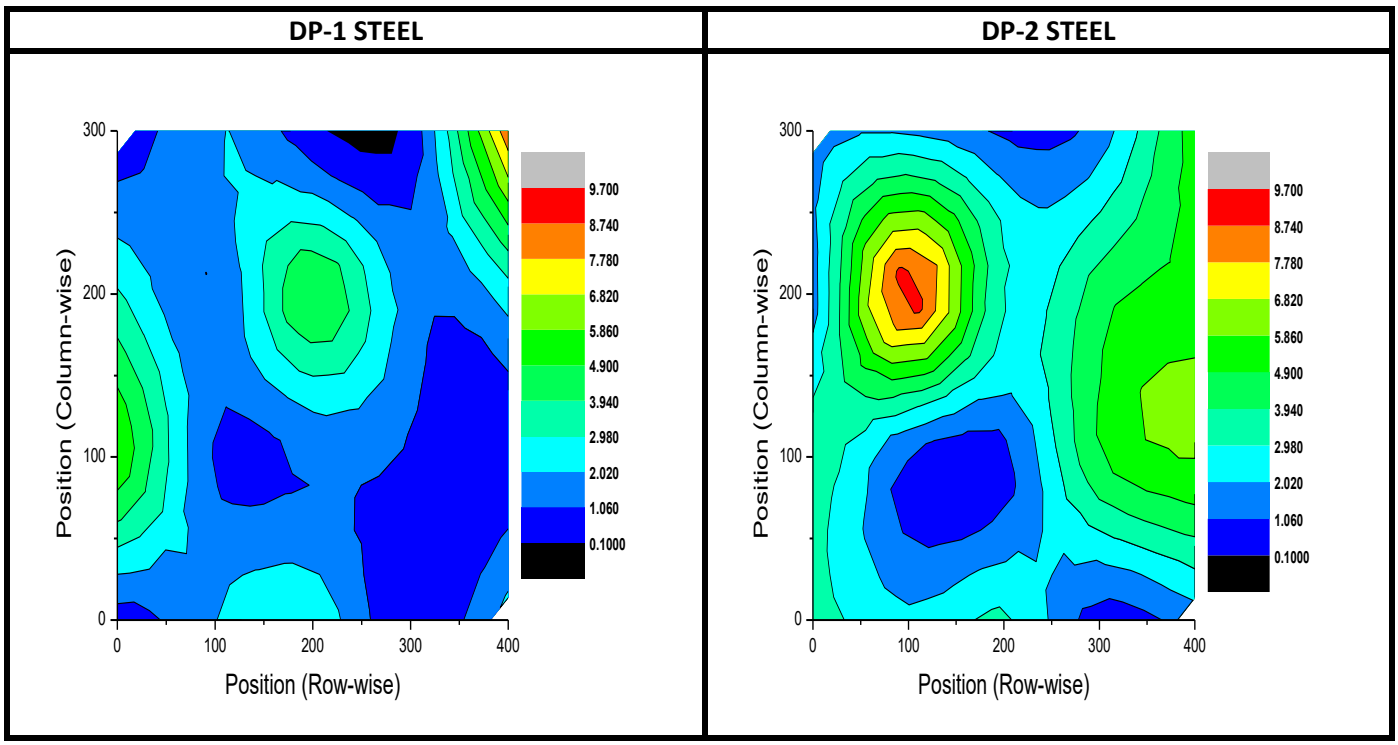

Figure 4.4 Contour plots showing variations in nano-indentation hardness values in load mode with regards to various layers for DP-1 and DP-2 steels.

Similar to the depth mode results (discussed in Section 4.4.1), contour plots for the load mode also showed even distribution of hardness values for DP-1 steels whereas wide variations in hardness were observed for DP-2 steels. Thus, nano-hardness evaluation in load mode also confirmed that in DP-1 steel, one of the two phases mainly underwent deformation whereas in DP-2 steel, both the phases actively participated in deformation which resulted in superior strength as well as ductility.

4.5 Spherical indentation results

This section describes the results of spherical indentation hardness testing. Figure 4.5 shows the image (using optical microscope) of spherical indentation for DP-1 steels.

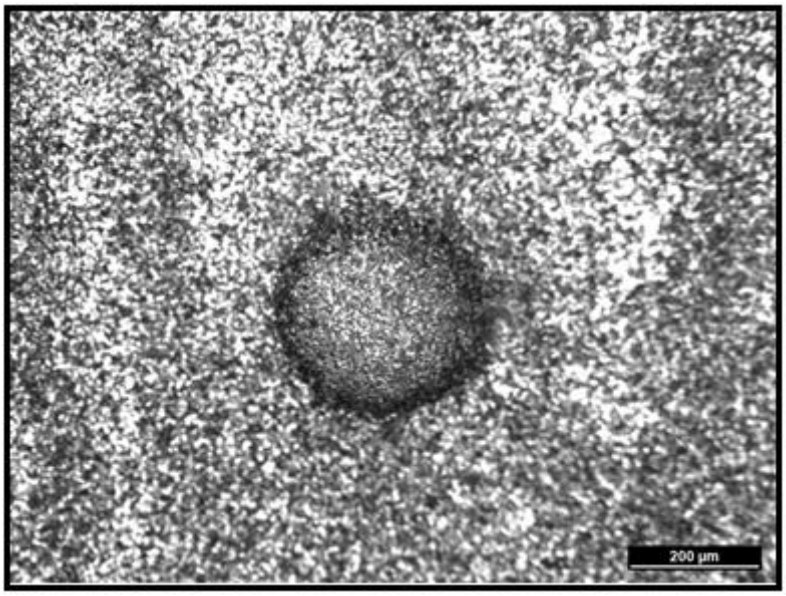

Figure 4.5 Image showing indentation mark on DP-1 steel after spherical indentation test.

For each steel, spherical indentation testing was done at two locations. For each location, hardness evaluation was done during progressive loading, with total loading/un-loadings as eight. Table 4.5 presents the results of spherical indentation hardness testing of DP-1 and DP-2 steels conducted in the depth mode.

Table4.5 Spherical indentation hardness values for DP-1 steel and DP-2 steel.

Physical position w.r.t to reference point (μm)	Matrix position (m×n)	Layer number (Unloading number)	Load, P (N)	Depth of indentation, h_c (microns)	Hardness (GPa)	Physical position w.r.t to reference point (μm)	Matrix position (m×n)	Layer number (Unloading number)	Load, P (N)	Depth of indentation, h_c (microns)	Hardness (GPa)
HARDNESS DATA FOR DP-1 STEEL											
LOCATION 1						***LOCATION 2***					
(0, 200)	1×3	1	148.8	10.6	2.93	(200,200)	3×3	1	150.1	10.6	2.98
		2	294.9	21.2	2.92			2	302.6	22.11	2.97
		3	412.8	29.9	2.90			3	454.5	32.95	2.93
		4	592.6	43.6	2.85			4	597.9	43.15	2.91
		5	744.7	54.9	2.85			5	745.9	53.93	2.90
		6	894.3	65	2.86			6	897.2	65.3	2.88
		7	1040.3	77.2	2.82			7	1042.4	76.7	2.85
		8	1187.8	88	2.81			8	1187.2	87.8	2.84
HARDNESS DATA FOR DP-2 STEEL											
LOCATION 1						***LOCATION 2***					
(0,200)	1×3	1	150.1	10.5	3.04	(200,200)	3×3	1	152	8.29	3.85
		2	298.8	21.2	2.94			2	300.6	18	3.38
		3	429.6	30.9	2.92			3	411.4	27.14	3.18
		4	593.1	43.2	2.87			4	600.7	39.89	3.16
		5	748.4	53.49	2.86			5	755.9	50.49	3.14
		6	891.8	63.56	2.86			6	890.3	60.28	3.1
		7	1045.1	74.65	2.87			7	1042.6	71.34	3.07
		8	1194.1	85.69	2.87			8	1198.3	83.08	3.03

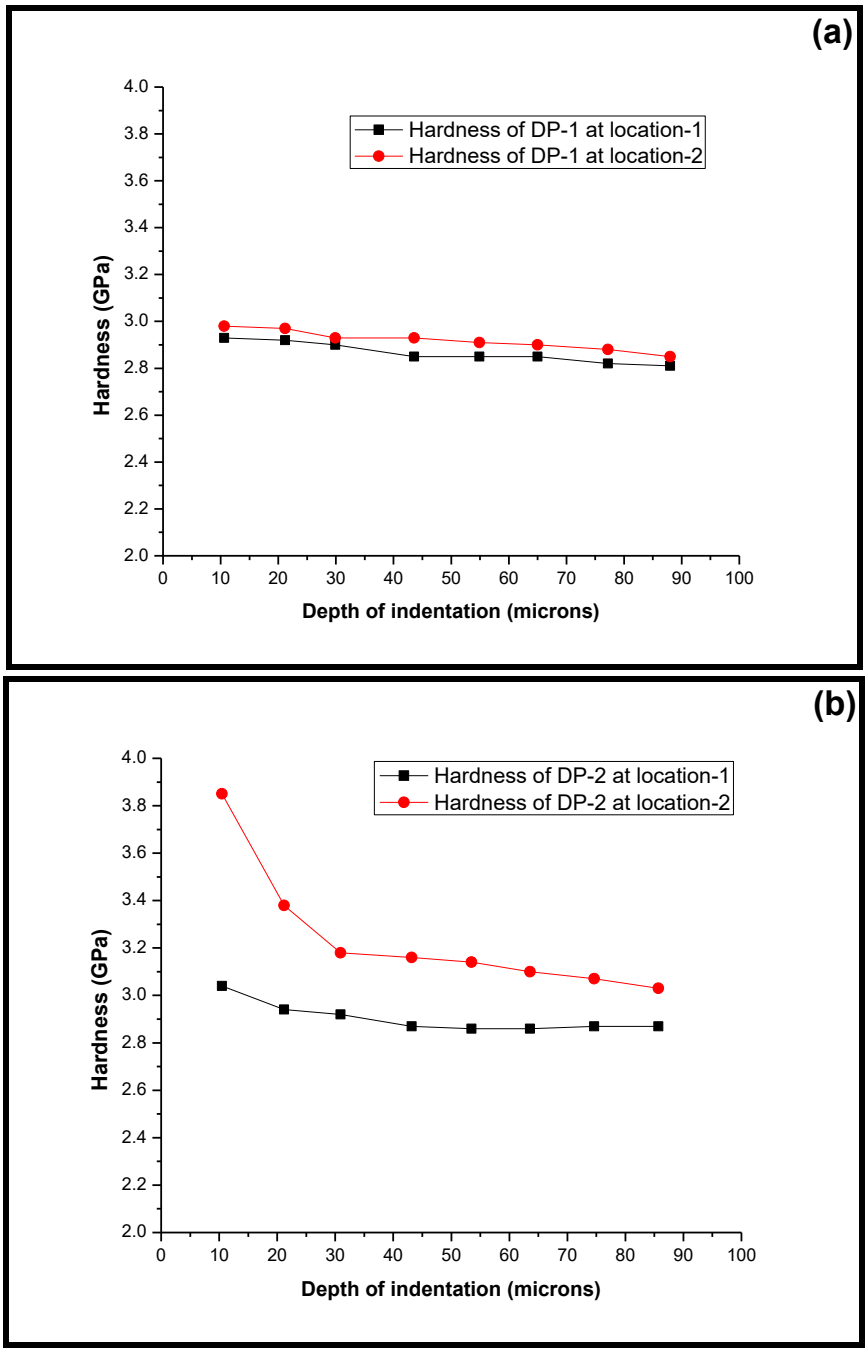

Figure 4.6 Plots showing variations in spherical indentation hardness values in depth mode with regards to various layers for (a) DP-1 steel, and (b) DP-2 steels.

The results of spherical indentation hardness testing bring forth the same conclusions as were drawn from the nano-indentation hardness testing results. For DP-1 steel, it can be observed from Figure 4.6a that hardness under a given condition remains almost same irrespective of the location

(i.e. hardness values at both the locations are almost the same under a given loading condition). On the contrary, for DP-2 steel, it can be observed from Figure 4.6b that hardness under a given condition varies significately at the two locations. These observations lead to the conclusion that for DP-1 steel, on application of load, only one of the phases present in the DP microstructure is participating in the deformation process. On the other hand, for DP-2 steel, since at different locations harness values ids different, it leads to the conculssion that both the phases are participating in the deformation process, resulting in relatively higher strength and higher ductility of DP-2 steels.

CHAPTER 5
CONCLUSIONS

5.1 General

This chapter presents the main conclusions to be drawn from the present dissertation work. It also presents the scope of future work.

5.2 Microstructure of the processed steels

- Harmonic structured dual phase steels were processed using CAS (core and shell) annealing route. Martensite core surrounded by ferrite shell was observed in the microstructures.
- Martensite volume fraction (MVF) in DP-1 and DP-2 steels was 52.2 % and 62.2% respectively. Martensite grain size was determined as 4.63 μm and 3.09 μm for DP-1 and DP-2 steels respectively.

5.3 Tensile properties of the processed steels

- DP-2 steel displayed better tensile properties than DP-1 steel. Ultimate strength and yield strength of DP-2 steel were observed as 1054 MPa and 637 MPa respectively as compared to 980 MPa and 570 MPa in DP-1 specimen respectively. DP-2 steel attained these higher strength levels than DP-1 steel with comparable value of percentage elongation.
- Superior properties were displayed by DP-2 steel because of the refined grain size of martensite which displayed better resistance to crack growth or better dampening of micro-cracks generated in martensite phase.

5.4 Nano-indentation hardness results

- Contour plots were made for the depth mode under progressive loading (0–450 mN; maximum depth of indentation: 3000 nm; loadings/un-loadings: 04; number of position points: 20; mode: for moderate to large depths) and also for the load mode (constant load: 0.5 mN; loading/un-loading: 01; number of position points: 20; mode: for shallow depths). This choice of diverse conditions (ranging from condition of low load of 0.5 mN to the condition of very high loads of 450 mN) for plotting contour plots permitted observation of hardness distribution

at the surface and also at greater depths from the surface for DP-1 and DP-2 steels. This hardness distribution helped in investigating contribution of microstructural features towards hardness. Thus, the output of contour plots represented the participation (or contribution) of micro-constituents of ferrite and martensite (of DP microstructure) in the deformation process during nano-indentation hardness testing (and hence also during tensile testing).

- For each layer of DP-1 steel, the contour plots showed more even distribution of hardness throughout the marked area. This signified that for DP-1 steel, only one of the two phases of DP microstructure was largely/significantly participating in the deformation process. On the contrary, for each layer of DP-2 steel, the contour plots were quite different with significant variations in hardness throughout the marked area (changes in colour throughout the plot). This signified that for DP-2 steel, both the constituent phases participated actively in the deformation process (e.g. the large volume fraction of blue region reflected presence of lower hardness phase of microstructure i.e. ferrite participation in deformation).
- Significant variations in hardness in the DP-2 steel also signified better distribution of secondary phase of microstructure around the primary phase or finer grain size of constituent phases, or both. Thus, because of the participation of both the constituent phases in the deformation process, DP-2 steel provided better strength and ductility as compared to DP-1 steel.
- Contour plots for the load mode also showed even distribution of hardness values for DP-1 steels whereas wide variations in hardness were observed for DP-2 steels. Thus, nano-hardness evaluation in load mode also confirmed that in DP-1 steel, one of the two phases mainly underwent deformation whereas in DP-2 steel, both the phases actively participated in deformation which resulted in superior strength with comparable ductility.

5.5 Spherical indentation results

- Hardness versus depth of indentation plots were made for the depth mode only under progressive loading (0–1200 N; loadings/un-loadings: 08; number of position points: 02).
- For DP-1 steel, (spherical indentation) hardness under a given condition remained almost the same irrespective of the location. On the contrary, for DP-2 steel, it was observed that hardness under a given condition varieed significately at the two locations. This showed that for DP-1 steel, on application of load, only one of the phase was participating in the deformation process.

For DP-2 steel, since at different locations, hardness values were different, both the phases were participating in the deformation process, resulting in relatively higher strength and higher ductility of DP-2 steels.

5.6 Major conclusions

- Dual phase steels processed through CAS route contain a typical harmonic type DP microstructure which provides good strength-ductility combination. Harmonic structured DP steels have very different microstructure compared to the conventional DP microstructure obtained through the industrial CAL route. The harmonic structured DP steels processed in the present work contained martensite as the primary phase (unlike conventional DP steels where ferrite is the primary phase). Martensite formed the core of microstructure surrounded by ferrite channel network as the shell. The presence of high martensite fraction in the processed steels ($> 50\%$), refined grain size of martensite ($<4.63\ \mu m$) coupled with presence of ferrite channel at the inter-martensite grain regions retarded the crack growth rate and prevented cracks from entering into adjacent martensite regions. These features provided good strength-ductility combination in the processed DP steels.
- Attempts to understand the tensile deformation behaviour of DP steels (ferrite-martensite dual phase microstructure) through hardness measurements were successful. Nano-indentation and spherical indentation test results showed that in a given DP microstructure, if hardness values vary in magnitude in different regions, it reflects that both phases of the microstructure have participated in the deformation process resulting in better strength-ductility combination. Thus, the present work clearly established the microstructure-hardness-tensile properties relationship in DP steels.

5.7 Scope for future work

In the present work, the two types of DP steels utilized contained harmonic structure with martensite as the primary phase. Microstructures of these two steels were different in terms of martensite fraction and grain size. The present work can be extended to compare the deformation/damage mechanisms in DP steels in which the primary phase is different (i.e. comparison of ferrite based steel with martensite based steel). In other words, steels processed through the conventional industrial CAL route can be compared with the CAS processed steels.

REFERENCES

1. P. Tsipouridis, H. Yoshida, S. Yonemura, S. Hiwatashi, S. Hirose, N. Suzuki, High strain rate properties of high strength steel sheets, *International Journal of Automobile Engineering* 2 (2011) 109–113.
2. E. Cadoni, N.K. Singh, M.K. Singh, N.K. Gupta, Strain rate behaviour of multi-phase and complex-phase steels for automotive applications, In: 10th International Conference on the Mechanical and Physical Behaviour of Materials under Dynamic Loading, Freiburg, Germany, 2nd–7th September, 2012, *EPJ Web of Conferences* 26, 05003 (2012).
3. J. Slycken, P. Verleysen, J. Degrieck, J. Bouquerel, Characterisation of the high strain rate properties of Advanced High Strength Steels, *High Performance Structures and Materials III* 85 259–268 (2006).
4. T. Nanda, V. Singh, V. Singh, A. Chakraborty, S. Sharma, Third generation of advanced high-strength steels: Processing routes and properties, *Journal of Materials Design and Applications* 1–30 (2016).
5. R. Kuziak, R. Kawalla, S. Waengler, Advanced high strength steels for automotive industry, *Archives of Civil and Mechanical Engineering* 8 103–117 (2008).
6. M. Mukherjee, T. Bhattacharyya, S.B. Singh, Models for austenite to martensite transformation in TRIP-aided steels: a comparative study, *Materials and Manufacturing Processes* 25(1–3) 206–210 (2010).
7. P. Simon, P.D. Beggs, A numerical performance comparison of a dual phase steel and aluminium alloy bumper bar system, *International Journal of Crashworthiness* 15 425–442 (2010).
8. Q.U. Hao, Advanced high strength steel through para equilibrium carbon partitioning and austenite stabilization. Ph. D. Dissertation, Case Western Reserve University, USA, 2011.
9. O.N. Cora, M. Koc, Promises and problems of ultra/advanced high strength steel (U/AHSS) utilization in automotive industry. In: The 7th Otomotiv Teknolojileri Kongresi (ed Solmaz E, Kaya N, Öztürk F), Bursa, Turkey, 26 May–27 May 2014, Uludag University, Bursa, 2014.
10. D.K. Matlock, J.G. Speer, "Processing opportunities for new advanced high strength sheet steels," *Materials and Manufacturing Processes* 25(1) 7–13 (2010).

11. D.K. Matlock, J.G. Speer, E.D. Moor, P.J. Gibbs, Recent developments in advanced high strength sheet steels for automotive applications: An overview, *Journal of Engineering Science and Technology* 15(1) 1–12 (2012).
12. S. Maggi, M. Murgia, Introduction to the metallurgic characteristics of advanced high strength steels for automobile applications, *Welding International* 22 610–618 (2008).
13. G. Weber, H. Thommes, H. Gaul, O. Hahn, M. Rethmeier, Mechanical properties of weld bonded joints of advanced high strength steels, *Journal of Adhesion Science and Technology* 25 2369–2389 (2011).
14. A. Uenishi, H. Yoshida, S. Yonemura, S. Hiwatashi, S. Hirose, N. Suzuki, High Strain Rate Properties of High Strength Steel Sheets, *International Journal of Automotive Engineering* 2 109-113 (2011).
15. H.G. Armaki, R. Maaßb, S.P. Bhat, S. Sriram, J.R. Greer, K.S. Kumar, Deformation response of ferrite and martensite in a dual-phase steel, *Acta Materialia* 2 197–211 (2014).
16. N. Saeidi, F. Ashrafizadeh, B. Niroumand, Development of a new ultra-fine grained dual phase steel and examination of the effect of grain size on tensile deformation behavior, *Materials Science and Engineering* A 599 145–149 (2014).
17. W. D. Nix and H. Gao, "Indentation size effects in crystalline materials: A law for strain gradient plasticity", *Journal of Mechanics and Physics of Solids*. 46, (3), (1998).
18. J. Kim, S. Kang, J. R. Greer, and D. Kwon, "Evaluating plastic flow properties by characterizing indentation size effect using a sharp indenter," *Acta Materilia* 56, 3338–3343, (2008).
19. K. Shinohara, I. K. Yasuda, and M. Yamada, "Universal method for evaluating work-hardening exponent of metals using ultra-microhardness tests," *Acta Materilia* 42, 3909–3915, (1994).
20. X. Chen, S. Lu, Y. Zhao, T. Fu, C. Huang, and X. Peng, "Molecular dynamic simulation on nano-indentation of NiTi SMAAuthor " *Material Science and Engineering A*, 712 592–602 (2018).
21. A. Das, M. Ghosh, S. Tarafder, S. Sivaprasad, D. Chakrabarti, Micro mechanisms of deformation in dual phase steels at high strain rates, *Material Science and Engineering A* 680 249–258 (2017).

22. P.D. Sudersanan, N. Kori, S. Aprameyan, U.N. Kempaiah, The effect of carbon content in martensite on the strength of dual phase steel, *International Journal of Industrial Engineering and Management Science* 2 (1–4) 2012.
23. H. ashrafi and R. E. N. Saeidi, "Correlation of tensile properties and strain hardening behavior with martensite volume fraction in dual-phase steels," *Transaction of Indian Institute of Metals*, 2016.
24. S. Sharma, T. Nanda, M. Adhikari, T. Venugopalan, V.R. Kumar, "A simulation study of pearlite-to-austenite transformation kinetics in rapidly heated cold rolled low carbon steel," *Materials and Design* 107 65–73 (2016).
25. Al-Abbasi, "Predicting the effect of ultrafine ferrite on the deformation behavior of DP-steels," *Computational Material Science* 119 90–107 (2016).
26. Concepción, N. Lorusso, G. Svoboda, Effect of carbon content on microstructure and mechanical properties of dual phase steels 8 1047–1056 (2015).
27. P. J. Jacques, T. Pardoen, and M. Delince, "Separation of size-dependent strengthening contributions in fine-grained dual phase steels by nanoindentation," *Acta Materilia* 54, 3395–3404, (2006).
28. A. Leitner and D. Kiener, "Dynamic nanoindentation testing : is there an influence on a material's hardness ?," *Materials Research Lletters* 3831, 486–493 (2017)
29. W.C. Oliver, G.M. Pharr, "An improved technique for determining hardness and elastic modulus using load and displacement sensing indentation experiments," *Journal of Materials Research* 7 1564–1583 (1992).
30. P. Gavendova and I. Petryshynets, "Dependence of grains hardness on their orientation in electrical steels," *Metal* (2–7), 2014.
31. N. Chollacoop, L. Li, and A. Gouldstone, "Errors in resolved modulus during nano-indentation of hard films on soft substrates : A computational study," *Material Science and Engineering A* 423, 36–40, (2006).
32. M. Singh, A. Das, T. Venugopalan, K. Mukherjee, M. Walunj, B.R. Kumar, T. Nanda "Impact of martensite spatial distribution on quasi-static and dynamic deformation behavior of dual-phase steel," *Metallurgical and Material Transactions A*, 49 463–475, (2018).

33. B.R. Kumar, N.K. Patel, K. Mukherjee, M. Walunj, G.K. Mandal, T. Venugopalan, Ferrite channel effect on ductility and strain hardenability of ultra-high strength dual phase steel, *Materials Science and Engineering A* 685 187–193 (2017).
34. Z. Gronostajski, A. Niechajowicz, R. Kuziak, J. Krawczyk, and S. Polak, "The effect of the strain rate on the stress-strain curve and microstructure of AHSS," *Journal of Material Process Technology*, 242, 246–259, (2017).
35. M. Erdogan and S. Tekeli, "The effect of martensite volume fraction and particle size on the tensile properties of a surface-carburized AISI 8620 steel with a dual-phase core microstructure," *Materials Characterization* 49, 445–454 (2003).
36. Z. Ma, S Long, Y. Pan, and Y. Zhou, "Indentation depth dependence of the mechanical strength of Ni films," *Journal of Applied Physics* 103 43512, (2008).